Received: 8 June 2020 | Revised: 10 July 2020 | Accepted: 14 July 2020

DOI: 10.1002/eom2.12047

REVIEW

EcoMat FUNCTIONAL MATERIALS FOR GREEN ENERGY AND ENVIRONMENT WILEY

Bi-based photocatalysts for light-driven environmental and energy applications: Structural tuning, reaction mechanisms, and challenges

Peng Chen[1,2] | **Hongjing Liu**[3] | **Wen Cui**[1] | **Shun Cheng Lee**[4] | **Li'ao Wang**[3] | **Fan Dong**[1,2]

[1]The Center of New Energy Materials and Technology, School of New Energy and Materials, Southwest Petroleum University, Chengdu, China

[2]Institute of Fundamental and Frontier Sciences, University of Electronic Science and Technology of China, Chengdu, China

[3]State Key Laboratory of Coal Mine Disaster Dynamics and Control, College of Environment and Ecology, Chongqing University, Chong Qing, China

[4]Department of Civil and Environmental Engineering, The Hong Kong Polytechnic University, Kowloon, Hong Kong

Correspondence
Fan Dong, Institute of Fundamental and Frontier Sciences, University of Electronic Science and Technology of China, Chengdu 611731, China.
Email: dfctbu@126.com, dongfan@uestc.edu.cn

Li'ao Wang, State Key Laboratory of Coal Mine Disaster Dynamics and Control, College of Environment and Ecology, Chongqing University, Chong Qing 400044, China.
Email: wangliao@cqu.edu.cn

Funding information
National Natural Science Foundation of China, Grant/Award Numbers: 21822601, 21777011; Graduate Research and Innovation Foundation of Chongqing, Grant/Award Number: CYS18019; The Graduate Research Innovation Fund Project of Southwest Petroleum University, Grant/Award Number: 2019cxyb012; 111 Project, Grant/Award Number: B20030

Abstract

Environmental pollution and energy crisis have become major challenges to sustainable development of human society. Solar-driven photocatalytic technology is regarded as an extremely attractive solution to environmental remediation and energy conversion. Unfortunately, practical applications of traditional photocatalysts are restricted owing to the poor absorption of visible light, insufficient charge separation and undefined reaction mechanism. Therefore, developing novel visible light photocatalysts and exploring their modification strategies are significant in the area of photocatalysis. Bi-based photocatalysts have attracted wide attention due to unique geometric structures, tunable electronic structure and decent photocatalytic activity under visible light. At present, Bi-based photocatalysts can be mainly classified as bismuth metal, binary oxides, bismuth oxyhalogen, multicomponent oxides and binary sulfides, and so forth. Although they can be used as independent photocatalysts for environmental purification and energy development, their efficiency is not ideal. Therefore, many efforts have been made to enhance their photocatalytic performance in the past few decades. Significant progresses in determining the fundamental properties of photocatalysts, improving the photocatalytic performance and understanding the photocatalytic mechanism in important reactions have been made benefited from the various new developed concepts and approaches. This review introduces the structural properties of Bi-based photocatalysts in detail and summarizes the design and modification strategy for improving the photocatalytic performance, including metal/

Peng Chen and Hongjing Liu contributed equally to this work.

nonmetal doping, construction of heterojunctions, regulation of crystal facet exposure, and structural defects. Furthermore, we discuss the catalysis mechanisms of Bi-based materials in terms of semiconductor photocatalysis and plasmonic photocatalysis. Finally, the applications, challenges and prospects of Bi-based photocatalysts are proposed to guide the future work.

KEYWORDS

Bi-based photocatalysts, energy conversion, environmental remediation, modification strategy, photocatalytic mechanism

1 | INTRODUCTION

With the rapidly developing of agriculture, industry and social economy, environmental pollution and the energy crisis have become major challenges to sustainable development of human society.[1-4] Solar-driven photocatalytic technology is an emerging photochemical technique and has been extensively studied since the 1970s. Photocatalysis can harvest energy directly from sunlight for water splitting into H_2 gas, harmful pollutant decomposition, selective organic transformations, N_2 fixation and CO_2 conversion to energy bearing carbon fuel sources.[5-9] Therefore, photocatalytic technology has been an extremely and environmentally friendly solution to environmental remediation and energy conversion.

The exploitation of photocatalysts is one of the keys to realize the high-performance application of photocatalytic technology.[10-12] Up to now, various semiconductor photocatalysts have been developed, including metal oxides (TiO_2, Bi_2O_3, etc),[13-16] metal sulfides (MoS_2, Bi_2S_3, etc),[17-21] multi-component oxides (Bi_2WO_6, $SrTiO_3$, etc),[22-25] metal selenides ($MoSe_2$, CdSe, etc),[26-29] metal phosphides (Co_2P, Ni_2P, etc),[30-32] metal phosphates (Ag_3PO_4, $BiPO_4$, etc),[33,34] metal halides (AgBr, etc),[35-37] metal oxyhalides (BiOBr, BiOCl, etc),[38-40] metal-free materials (SiC, g-C_3N_4, etc)[41-43] and so on. Among them, the semiconductor with a band gap of Eg $\geq$ 3 eV are called wide-band-gap photocatalysts. On the contrary, those with a band gap of Eg $\leq$3 eV are called visible-light-responsive photocatalysts.[44] The wide-band-gap photocatalysts can only be stimulated by high-energy ultraviolet light that accounts for less than 5% of incident solar light.[45] Nevertheless, the energy of visible light accounts for 43% in solar energy and thus developing visible-light-responsive photocatalysts are necessary in photocatalysis.

Among reported semiconductor photocatalysts, a variety of visible light active Bi-based photocatalysts has recently received considerable interests. Researches indicates that the stability of Bi^{3+} is better than that of Bi^{5+} and thus Bi^{3+}-containing compounds have been studied more extensively rather than Bi^{5+}-containing compounds. In the valence band of Bi^{3+}-containing compounds, overlap of O *2p* and Bi *6s* orbitals could enhance the photogenerated charge mobility for improving the photocatalytic activity. Additionally, the band gaps of most Bi-based compounds are usually small and can be excited by visible light except for BiOF, BiOCl or $Bi_2O_2CO_3$ etc.[46-48] Therefore, Bi-based photocatalysts have attracted intensive research interests on environmental remediation and energy conversion.

Plentiful Bi-based photocatalysts have recently been reported including Bi metal, Bi_2O_3, BiOCl, $Bi_2Ti_2O_7$, Bi_2WO_6, $Bi_2O_2CO_3$, Bi_2S_3, etc. And they can usually be categorized as bismuth metal, binary oxides, bismuth oxyhalogen, multi-component oxides and binary sulfides. However, the photocatalytic performance of those individual Bi-based semiconductors is not sufficiently effective for practical environmental and energy applications due to the excessive electron-hole recombination and the limited absorption ability of visible light. Many attempts have been made to improve the photocatalytic efficiency of pure Bi-based photocatalysts, which concentrated on doping, heterojunction construction, crystal plane regulation and defect structure. Additionally, the photocatalytic mechanisms of Bi-based photocatalysts have not been deeply discussed in environmental remediation and energy conversion. Considering the rapid development of this important area, a comprehensive review is necessary to summarize the recent advances on Bi-based photocatalysts. In this review (as shown in Figure 1), the research progress of bismuth-based nanophotocatalytic materials is introduced in detail based on the structure properties, the photocatalytic mechanism, and design strategy for enhancing light-driven Bi-based photocatalytic performance. Finally, the developments, challenges and prospects of Bi-based photocatalysts are summarized in environmental and energy applications.

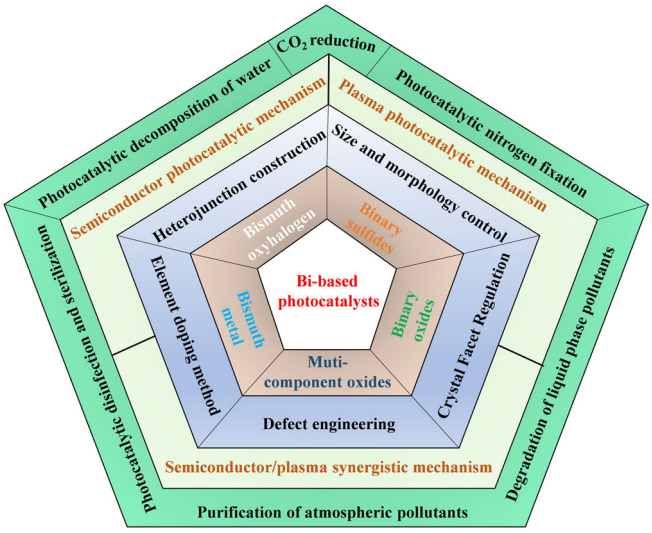

FIGURE 1 Schematic illustration of Bi-based photocatalysts for light-driven environmental and energy applications

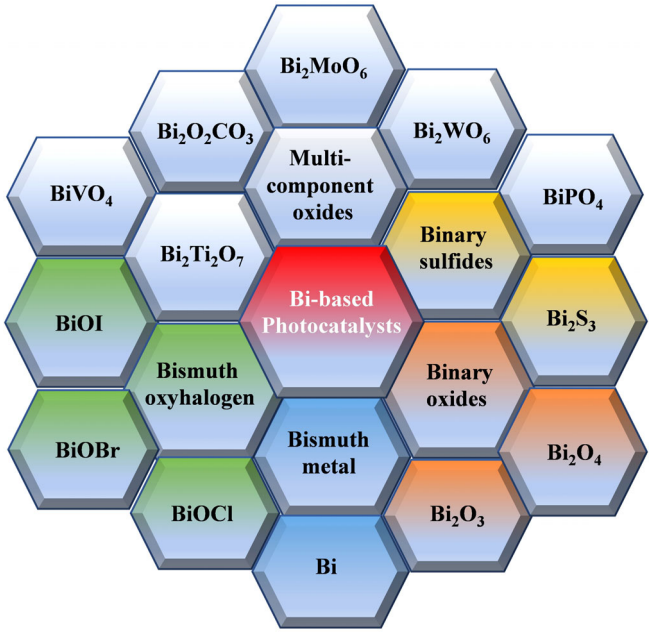

FIGURE 2 Schematic illustration of classify and partial chemical formulations for Bi-based photocatalysts

2 | STRUCTURAL OF BISMUTH-BASED PHOTOCATALYTIC MATERIALS

Many Bi-based photocatalysts have recently been developed as shown in Figure 2. Most of Bi-based photocatalysts can be excited via visible light owing to a band gap of less than 3.0 eV, except for BiOF, BiOCl, and $Bi_2O_2CO_3$ etc. Additionally, Bi_2S_3, BiOI, and $KBiO_3$ can absorb visible light with longer wavelengths because of a band gap (<2.0 eV). The band gap will affect the light absorption capacity and also determine the generation of carriers. Moreover, the photocatalytic activity is also affected by their electronic structures and band positions, which will determine the separation and migration of carriers and the redox reaction. Therefore, the structure properties of Bi-based photocatalysts have been extensively investigated.

2.1 | Bismuth photocatalyst

The bismuth (Bi) in ground state has a rhombohedral A7 trigonometric symmetric structure (space group No. 166, $R\bar{3}m$). [49,50] That structure comes from the transformation of simple cubic structure via two separate distortions including trigonal shear and relative displacement.[51-53] Moreover, mosaic structures of Bi consisted of one monoclinic (M) and two triclinic structures (T1 and T2).[54] They might be formed through the tiny lattice distortion of A7 structure and they coexist with the A7 structure.[55] Wu et al reported the structures of Bi including A7, M, T1, and T2 in Figure 3A. The No. 166 ($R\bar{3}m$), No. 12 (C2/m), No. 2 ($P\bar{1}$), and No. 2 (P1) in space groups were assigned to A7, M, T1, and T2 structures, respectively.[54,56,57] The unique electronic band feature of Bi is the existence of a small overlap between conduction band at the L points of the Brillouin zone and valence band at the T points (T and L points would have been equivalent in nondistorted f.c.c lattice). That overlap is attributed to the semimetallic character of Bi. Gonze et al developed the band structure of the A7 structure of Bi.[58] Additionally, Wu et al also pointed to that the M-phase Bi is a semimetal similar to the A7-phase Bi.[49,59] And some studies have shown the semimetallic property is existed in T1-phase Bi and also found the band gap of direct semiconductor T2-phase Bi is narrow (0.07941 eV).[49] Among them, the T2-phase Bi has better thermoelectric properties.[49] The classification of Bi as a semimetal is closely related to its unique properties including very special electronic structure, small effective masses, long Fermi wavelength, etc. Additionally, a transition from semimetal to semiconductor would be happed in the Bi with diameters of several tens of nanometers due to the nanoconfinement effects.[60-65]

Moreover, Bi has been found to exhibit plasmonic properties similar to Au and Ag. The collective stimulation of the free electrons in the semimetallic Bi results in the SPR phenomenon, which leads to the strongly resonant light absorption and the enhancement of near-field and scattering.[66,67] This implies that bismuth has good absorptivity either as a semimetal with plasma resonance effect or as a material with semiconductor property, but how to control the particle size and size of bismuth and

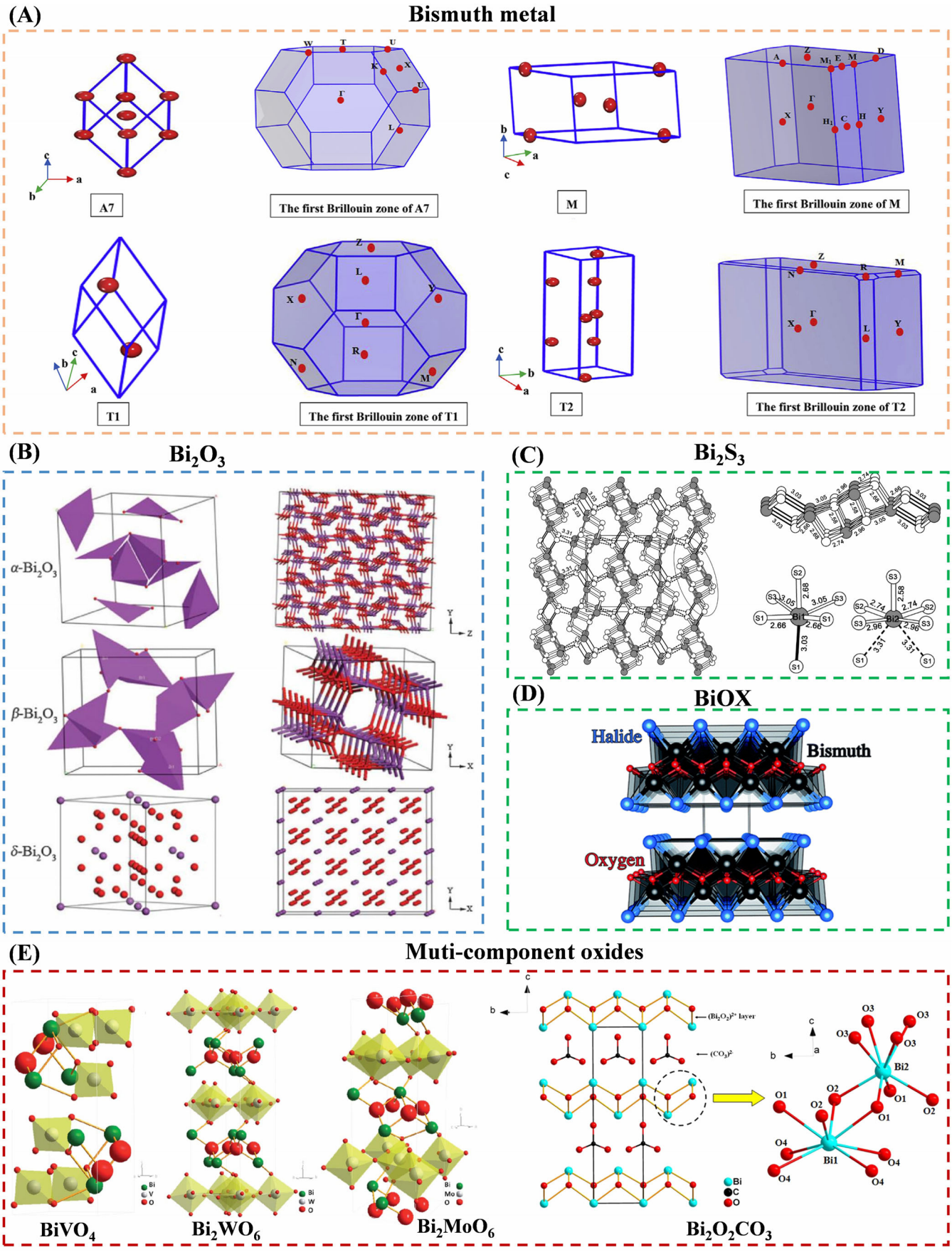

FIGURE 3 Legend on next page.

study the semimetallic properties or plasma resonance effect of bismuth and its photocatalytic performance relations need further in-depth study in the same system.

2.2 | Bismuth oxide and sulfides photocatalyst

Bi_2O_3 has six crystal forms of α, β, γ, δ, ε, and ω.[68,69] The typical crystal types are α-, β-, γ-, and δ-Bi_2O_3. Figure 3B shows the crystal structures of some Bi_2O_3. Among them, α-Bi_2O_3 (monoclinic structure) and δ-Bi_2O_3 (face-centered cubic structure) are respectively the stable phases of low temperature and high temperature. The β-Bi_2O_3 (tetragonal structure) and γ-Bi_2O_3 (body-centered cubic structure) are metastable phases. Different crystalline phases can be transformed into each other at a certain temperature. Bi_2O_3 has α phase at room temperature and its melting point is 824°C. It can be transformed into δ phase when it is heated to 729°C. In the process of cooling, the δ phase will precipitate to form β phase and γ phase at 650°C and 639°C, respectively.[70] Oxygen vacancies in the structure of δ-Bi_2O_3 are irregularly distributed. Oxygen ions in the structure have high mobility, which shows high conductivity of oxygen ions.[71] The arrangement of oxygen vacancies in the structures of β-Bi_2O_3 and δ-Bi_2O_3 is similar. The band gap of Bi_2O_3 is widely distributed during 2.1 to 3.96 eV,[72,73] the band gap energy of β-Bi_2O_3 is 2.58 eV and α-Bi_2O_3 is 2.85 eV. Due to the various crystal types and wide adjustable band gap width, Bi_2O_3 exhibits high-performance oxygen ion conductivity, excellent dielectric property, high refractive index, excellent photoconductivity and photoluminescence performance depending on their phase structure. Therefore, Bi_2O_3 is widely used in optoelectronic materials, sensors, microelectronic components, catalysis, high temperature superconducting materials and high refractive index glasses and other fields.[74]

As a visible-light photocatalyst, Bi_2O_3 shows excellent photocatalytic performance and has huge potential application prospects in the field of photocatalysis. However, due to its inherent drawbacks such as poor structural stability, prone to photocorrosion, and high loading rate of photogenerated electron holes, Bi_2O_3 is not used as a catalyst alone to degrade organic pollutants.[75,76] Therefore, the current research focuses on improving the structural stability of Bi_2O_3, improving its light corrosion resistance and enhancing its visible light response. In addition, the photocatalytic mechanism of Bi_2O_3 heterojunction complex, the interfacial properties, loading properties, recycling, and the combination of different composite modification methods are still worthy of further study.

Besides Bi_2O_3, bismuth oxides also contain monoclinic dibismuth tetraoxide (m-Bi_2O_4) which has recently attracted the attention of scholars in the field of photocatalysis due to its excellent visible light absorption and unique electron band structure.[77-80] Wang et al prepared submicrorods m-Bi_2O_4 with a narrow band gap (2.0 eV), which wavelength of light absorption up to 620 nm and also show an excellent visible-light photocatalytic activity for degradation of organic pollutants and bacterial inactivation.[79] Herein, m-Bi_2O_4 might be a novel and stable photocatalyst with visible-light response, which will have great application prospects in the fields of environmental restoration and energy conversion. However, the current research about preparation technology, morphology regulation, and electronic structure adjustment of m-Bi_2O_4 are still insufficient, so future research work can focus on the above aspects to further develop and develop advantages of m-Bi_2O_4.

Bi_2S_3 is a typical $A_2^{V}B_3^{VI}$ (A = As, Sb, Bi; B = S, Se, Te) metal chalcogenide compound, which has a narrow band gap during 1.3 to 1.7 eV. And Bi_2S_3 crystal is usually orthorhombic phase with a lamellar structure.[81,82] Figure 3C shows the crystal structure characteristics of Bi_2S_3. Along the b axis, the pseudolayer is weakly connected via Bi2-S1 = 3.31 Å interactions. Additionally, each pseudolayer contains $[Bi_4S_6]_\infty$ ribbons that is constructed by Bi-S bond in 2.58 to 2.74 Å. The Bi1 is 6-fold coordinated with three strong Bi-S bonds and three weak ones. And Bi_2 has a 5-fold coordinated square pyramid sphere.[83] To date, much effort have been focused on the synthesis of various Bi_2S_3 nanostructures such as nanorods, nanoribbons, nanowires, nanoflowers, and nanocabbages by different methods including template-directed method, hydro/solvothermal procedure, microwave irradiation, electrochemical deposition, and sonochemical techniques.[83-85] Bi_2S_3 is easily stimulated by visible light to

FIGURE 3 A, Four polytype phases of Bi and their corresponding first Brillouin zones. B, Crystal structure of Bi_2O_3 crystal form: α-Bi_2O_3, β-Bi_2O_3, δ-Bi_2O_3. C, Single crystal structure of Bi_2S_3. D, The BiOX crystal structure. E, Schematic crystal structure of $BiVO_4$, Bi_2WO_6, Bi_2MoO_6, and $Bi_2O_2CO_3$ in the mode: scheelite $BiVO_4$, Aurivillius orthorhombic Bi_2WO_6, Aurivillius orthorhombic Bi_2MoO_6. orthorhombic $Bi_2O_2CO_3$. *Source*: A, Reproduced with permission: Copyright 2019, Elsevier.[49] *Source*: B, Reproduced with permission: Copyright 2010, Royal Society of Chemistry.[114] *Source*: C, Reproduced with permission: Copyright 2009, American Chemical Society.[83] *Source*: D, Reproduced with permission: Copyright 2016, Royal Society of Chemistry.[86] *Source*: E, Reproduced with permission: Copyright 2014, Royal Society of Chemistry.[101] Copyright 2014, Elsevier[102]

produce electron-hole pairs, which makes it a potential material for photocatalytic environmental remediation and energy conversion. But the practical applications of Bi_2S_3 as a single catalyst is limited due to its inherent defects, such as poor structural stability, prone to photoetching, and high load rate of photoelectron holes.

2.3 | Bismuth oxyhalogen photocatalyst

2.3.1 | Crystal structure

The crystal structure of BiOX (X = F, Cl, Br, I) is PbFCl type with D4h symmetry and *P4*/nmm space group, and BiOX belongs to tetragonal system. As shown in Figure 3D, $[Bi_2O_2]^{2+}$ layer interlaces with double halogen ions in the crystal structure of BiOX, which makes BiOX material have strong anisotropy.[48,86] The [X-Bi-O-Bi-X] layer of BiOX is extended along (001) direction, and the layer with positive charge and the [X] layer with negative charge can induce an internal electric field along (001) direction.[70] And BiOX has an asymmetric decahedral geometry owing to the special coordination around bismuth center in each [X-Bi-O-Bi-X] layer.[87] Interactions in the $[Bi_2O_2]^{2+}$ layer are generated by covalent bonds, while the [X] layer is superimposed by van der Waals forces (nonbonding interactions) between X atoms along the c axis.[39] The formation of layered structures can be induced by covalent bonding in strong layers and van der Waals interaction between weak layers. Under the action of internal electric field, the photogenerated electron-hole pairs produced by photoexcitation can be easily separated, which is helpful to the photocatalytic reaction.[88-91]

2.3.2 | Electronic structure

For BiOX crystal, the composition of O 2p state and X np state (X = Cl, Br and I are n = 3, 4, and 5 respectively) constitutes the valence band maximum, and the conduction band minimum is dominated by Bi 6p state.[39,92-94] When the atomic numbers of X increases, the band gap will be narrowed and the dispersive characteristic of band energy level becomes more obvious due to the significantly increasing contribution of X ns states. Obviously, the composition of the layered structure such as atomic numbers of X can highly affect the band gap values and the redox potentials of BiOX. In the BiOX series of semiconductors, BiOF is direct bandgap semiconductor with large band gap and is less studied. BiOCl, BiOBr and BiOI are all indirect bandgap transitions. The three semiconductors (BiOCl, BiOBr and BiOI) show different advantages and disadvantages in photocatalytic applications. The band gap of BiOCl is about 3.2 eV, so the absorption threshold of BiOCl is in the ultraviolet region and the absorption ability of BiOCl to visible light in sunlight is weak. The band gap width of BiOBr is about 2.9 eV and the response range to visible light is relatively low. The band gap of BiOI is the smallest, showing a high absorption capacity of visible light. But the redox ability of BiOI in the photocatalytic process is weak due to the redox potential position problems of valence band and conduction band, which limits its photocatalytic application. Therefore, BiOX photocatalytic materials need further modification to achieve higher photocatalytic activity and expand its practical application.

2.4 | Multi-component oxides photocatalyst

Bi-based multi-component oxides contain various oxysalts including $BiVO_4$, $Bi_2Ti_2O_7$, $Bi_2O_2CO_3$, Bi_2WO_6, and Bi_2MoO_6, etc., usually with a layered Aurivillius structure, that is, . $[Bi_2O_2]^{2+}$ layers inter-grown along the c axis. In this section, we focus on the mostly studied $BiVO_4$, $Bi_2O_2CO_3$, Bi_2WO_6, and Bi_2MoO_6 materials.

2.4.1 | Crystal structure

$BiVO_4$ mainly has three crystal structures including tetragonal scheelite structure, monoclinic scheelite structure and tetragonal zircon structure. Different crystal forms can be transformed with each other under certain conditions.[95] At high temperature, the tetragonal phase of $BiVO_4$ is a stable phase. In addition, the phase transition was reversible between monoclinic scheelite $BiVO_4$ and tetragonal scheelite $BiVO_4$ at 528 K.[96] The band gap of tetragonal zircon $BiVO_4$ is 2.9 eV and the scheelite $BiVO_4$ has a band gap of 2.4 eV. At present, the scheelite $BiVO_4$ is the most widely studied $BiVO_4$ photocatalyst.[97] Figure 3E exhibits the crystal structure of scheelite $BiVO_4$. The Bi-V-O units stacked to form a layer structure parallel to the c axis. A VO_4 tetrahedron is formed via coordination between one V ion and four oxygen atoms. Each VO_4 tetrahedron is not in contact with each other and each Bi ion interacts with eight oxygen atoms in eight different VO_4 tetrahedron.[98]

Bi_2MO_6 (M = Mo, W) have two crystalline phases in compounds: orthorhombic and monoclinic structure. At a low and medium temperatures ($T < 960^\circ C$), the orthorhombic structures of Bi_2MoO_6 and Bi_2WO_6 were mainly formed while the monoclinic structure existed at a high temperature ($T > 960^\circ C$).[99,100] The orthorhombic phase of Bi_2MO_6 (M = Mo, W) photocatalyst has been studied widely. Figure 3E exhibits the schematic crystal structure of

the orthorhombic Bi_2WO_6 and Bi_2MoO_6, respectively. A layered structure can be observed in Bi_2MO_6 (M = Mo, W) photocatalysts, which consists of MO_6 octahedral layers and Bi-O-Bi layers. Each MO_6 octahedron is connected to each other through corner-sharing O atom. The $[Bi_2O_2]^{2+}$ layers are sandwiched between MO_6 octahedral layers.[100,101] $Bi_2O_2CO_3$ is a typical "Aurivillius" phase in which the $[Bi_2O_2]^{2+}$ layer and $[CO_3]^{2-}$ layer are symbiotic in an orthogonal manner, forming a two-dimensional structure. The $Bi_2O_2CO_3$ crystallizes in the orthorhombic space group Imm2. The crystal structure was shown in the left of Figure 3E. The segregated "standing-on-end" carbonate layer can be clearly seen in the crystal structure and the two kinds of Bi atoms are all eight coordinated.[102,103]

The $BiVO_4$, Bi_2MoO_6, Bi_2WO_6, and $Bi_2O_2CO_3$ photocatalysts generally have a layer structure with local lattice distortions that derived from asymmetric coordination environments drived by Bi 6s lone pair electrons. In addition, the electronic structure would be affected by the distortion of the local crystal structure, which would affect the photocatalytic activity.

2.4.2 | Electronic structure

The $BiVO_4$, Bi_2MoO_6, and Bi_2WO_6 photocatalysts possess a direct band gap. According to density functional theory (DFT) calculations, the O 2p and Bi 6s levels form the valence band while M nd (V 3d, Mo 4d, W 5d) levels form the conduction band, which demonstrates that the charge in O 2p + Bi 6s hybrid orbitals would transfer to the empty M nd orbitals during photoexcitation.[104-108] In addition, the Bi $6s^2$ lone pair with spatial activity reduced the oxidation band gap and improved the hole conductivity, because the Bi 6s orbital was located in the O 2p orbital and dispersed the top of the valence band to a large extent.[106] In combination with the analysis of crystal structure and electronic structure, M is generally considered to be a reduction site while oxidation may occur at Bi or O sites[109] $Bi_2O_2CO_3$ has an indirect band gap about 3.1 eV.[110-112] The conduction band is mainly composed of Bi 6p states while the O 2p, C 2p and Bi 6s states form the valence band, and the band-gap transition mainly occur between O 2p states and Bi 6p states. Moreover, the O 2p states form the gap states below the Fermi level, which is from the $[CO_3]^{2-}$ units but not the $[Bi_2O_2]^{2+}$ layers. Some discrete states composed of C 2p and O 2s states are also introduced via $[CO_3]^{2-}$ units, which lie below the valence band bottom. Compared to $[CO_3]^{2-}$ units, the contribution of O 2p from $[Bi_2O_2]^{2+}$ layers to the gap states is little and the O 2s states of $[Bi_2O_2]^{2+}$ layers are not discrete.[113]

3 | STRUCTURAL TUNING OF BISMUTH-BASED PHOTOCATALYTIC MATERIALS

Up to now, the photocatalytic performance of pure Bi-based semiconductors is not active sufficiently for practical environmental and energy applications because the limited absorption ability of visible light and the excessive recombination of electron-hole pairs. According to the understanding on structure properties of Bi-based photocatalysts in Section 2, the crystal structure and electronic structure of semiconductors would affect photocatalytic activity. From the perspective of crystal structure, the photocatalytic performance is strongly linked to the size, morphology, and crystal facet of Bi-based photocatalysts. Therefore, photocatalytic properties could be enhanced by controlling the photocatalyst microstructure. Additionally, the electronic structure can control many properties of photocatalysts including the light absorption properties, charge separation and transfer, thermodynamic and kinetic processes of photocatalytic reactions. Recently, many strategies have been made to regulate electronic structure to enhance the photocatalytic performance, which include doping, heterojunction construction, crystal plane regulation and defect structure. This section will outline these strategies used to regulate the structures of Bi-based photocatalysts and discuss how they affect the photocatalytic performances.

3.1 | Microstructure control

3.1.1 | Size and morphology control

Photocatalysts may exhibit different properties when reducing the dimension to nanoscale. A significant increase in the percentage of atoms or ions exposed to catalyst surface will result in largening specific surface area, thus promoting the increase number of active sites for the photocatalytic reactions.[115-117] Under light irradiation, average diffusion time of photogenerated carrier from bulk to surface can be given by $\tau = r^2/\pi^2 D$, where r is the grain radius and D is the diffusion coefficient of the carrier.[118] Therefore, when particle radius is reduced, abundant photogenerated carriers would be easily moved to the surface for photocatalytic reaction. Bismuth as a plasmonic photocatalyst is generally in the nanoscale range. Many methods can be used to synthesize nanospheres, nanorods and nanosheets.[119-121] Figure 4A shows typical synthetic methods of bismuth, which can be controlled by adding surfactants such as PVP and citric acid.[122] It was found that Bi nanostructures in various morphology extended different optical properties. The

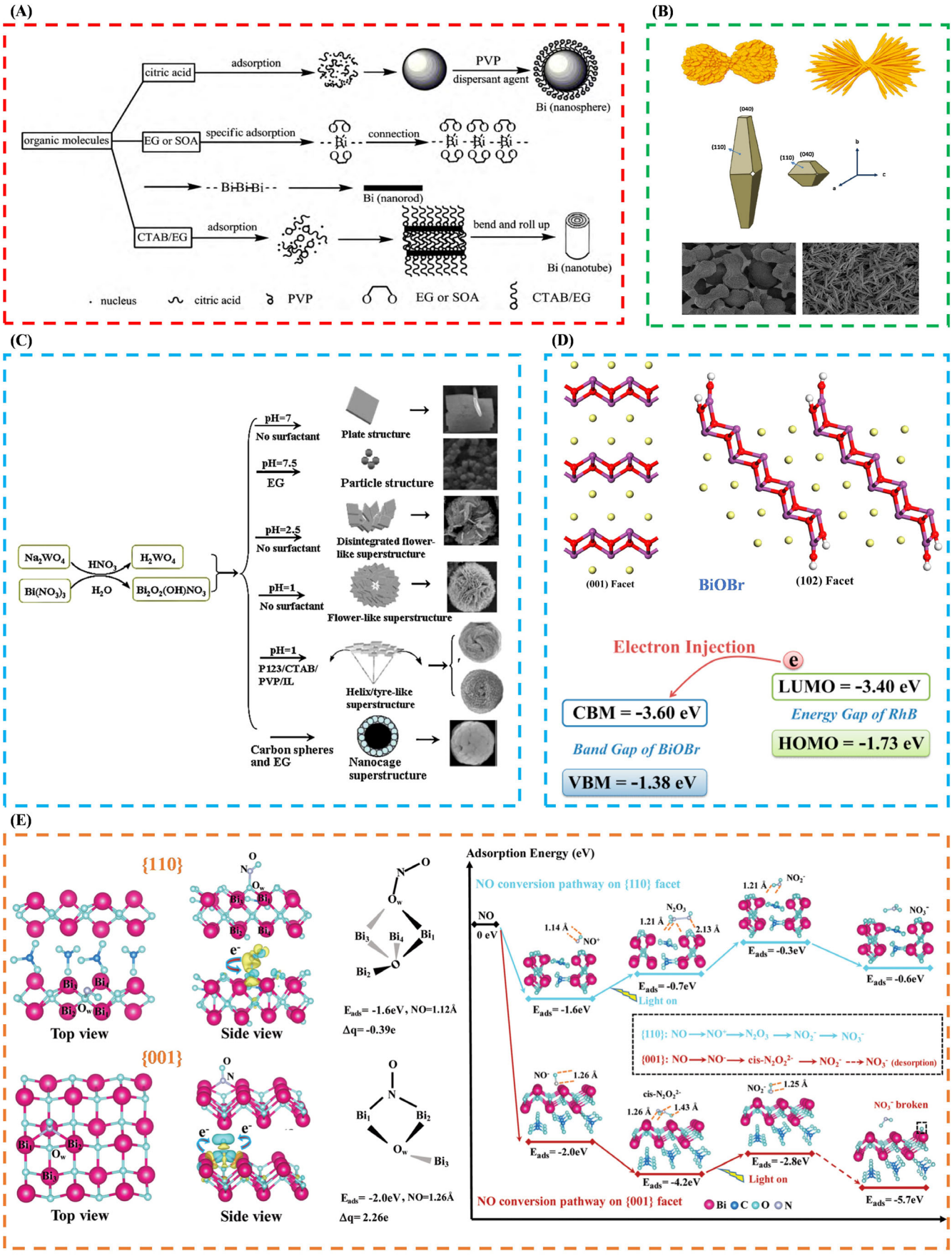

FIGURE 4 Legend on next page.

absorption peaks in UV-visible spectra were shifted or broadened owing to the decreased sizes or the changed shapes of the synthesized Bi nanostructures. It is reported that the surface plasmon resonance (SPR) absorption peaks of bismuth (Bi) are in the range of 230 to 290 nm, which will change with the size and shape of Bi. Therefore, the SPR effect can be modulated by adjusting the size and shape of Bi metal nanoparticles. The results show that the increase of bismuth particle size (>100 nm) may lead to new absorption peaks during 300 to 600 nm, which may be attributed to the scattering of bismuth. In a few studies on bismuth, bismuth is observed as the absorption edge of semiconductors with narrow band gap below 2.5 eV. This shows that bismuth has good absorptivity either as a semimetal with plasma resonance effect or as a material with semiconductor property.[119-121]

Additionally, the morphologies of photocatalysts also affect the catalytic performances. Several $BiVO_4$ samples with peanut-like and needle-like architectures have been synthesized (Figure 4B).[123] The needle-like $BiVO_4$ showed better photocatalytic performance, which indicates the morphology of prepared $BiVO_4$ strongly affected the photocatalytic activity. In addition, the parameters such as pH values, surfactants and/or template would affect the synthesis processes of photocatalyst and thus determining their morphologies. The different shapes of Bi_2WO_6 samples have been synthesized by tuning above parameters, which includes nanoplates, nanoparticles, and flower/sphere-like, nest/tyre/helix-like and nanocage-like superstructures, summarized in Figure 4C.[124-129] The different morphologies of Bi_2WO_6 have obtained different structure properties related to the photocatalytic performance. Therefore, when those Bi_2WO_6 were applied to degrade the organic pollutant and disinfect the bacteria, they exhibit structure/component-dependent photocatalytic performance.

The above progress has demonstrated that size and morphology of Bi-based photocatalyst plays a crucial role in photocatalysis. However, it is worth noting that the increased specific surface area by reducing the size or changing morphology also means that the carrier recombination is more likely to appear on the surface. When the recombination plays a major role, the activity will also decrease. Therefore, attention should be paid to balance the effect of the structural properties caused by the size and morphology on the photocatalytic reactivity in the actual photocatalytic process. It is a significant direction to improve photocatalytic performance of Bi-based photocatalysts by developing precise regulation means or methods to obtain the best catalytic active sites and specific surface area, etc.

3.1.2 | Crystal facet regulation

The surface atom arrangement and coordination of semiconductor photocatalysts directly determine their adsorption and desorption performance and the surface migration of photogenerated carriers, the photocatalytic efficiency will be affected by the surface state of the catalyst. Surface atom alignment and coordination change is reflected by the crystal surface of semiconductor with different orientation. Therefore, for a specific semiconductor photocatalyst, different exposed crystal surfaces strongly affect its photocatalytic performance.[130-132]

Recently, some researchers reveal that a semiconductor exposed to particular plane has a lower conduction band and a higher valence band, thereby narrowing the band gap and facilitating the generation of electron-hole pairs under light irradiation. For instance, Zhang et al compared the photocatalytic properties of BiOBr respectively exposed (102) and (001) facets (Figure 4D).[130] The study found that the BiOBr exposed (102) facet has a lower minimum value of conduction band and a maximum value of higher valence band compared with the BiOBr exposed (001) facet owing to the different surface states. Therefore, BiOBr with exposing (102) facet has higher electron injection efficiency, thus having better photocatalytic performance. In addition, the exposure of specific crystal surface in the photocatalyst can facilitate the electron-hole pair charge separation, and thus showing higher photoreactivity. Ye et al reported that the density of oxygen atoms in {001} crystal surface of BiOCl is high, so abundant oxygen vacancies will be generated under ultraviolet irradiation, thus improving the electron-hole separation efficiency, and enhancing the photoactivity of BiOCl.[132] Additionally, the formation mechanisms of facet-dependent radicals and pollutant

FIGURE 4 Microstructure control. A, The influence of different surfactants on the different morphology preparation of bismuth monomer. B, Schematic illustration of different morphologies of $BiVO_4$. C, The summary diagram of different morphologies of Bi_2WO_6 by adjusting pH value or adding different surfactants. D, Structures of BiOBr with different facets and illustration of electron injection of the RhB-BiOBr system. E, The different NO adsorption models on the {110} and {001} surfaces of $Bi_2O_2CO_3$. *Source*: A, Reproduced with permission: Copyright 2010, Elsevier.[122] *Source*: B, Reproduced with permission: Copyright 2012, Elsevier.[123] *Source*: C, Reproduced with permission: Copyright 2011, Elsevier.[124] *Source*: D, Reproduced with permission: Copyright 2014, American Chemical Society.[130] *Source*: E, Reproduced with permission: Copyright 2019, Royal Society of Chemistry[131]

adsorption activation mechanism of different facets, which could result in enhanced catalytic activities.[131] Chen et al pointed out that the interactions between different crystal surfaces and the adsorption reactants were different, which leads to the different adsorption and activation mechanisms of the reactants that would have a significant impact on the photocatalytic activity and reaction mechanism (Figure 4E). Additionally, activation of O_2 and H_2O molecules on $Bi_2O_2CO_3$ with {001} exposure (denote as 001-BOC) are stronger, so more active free radicals are stimulated to promote photocatalytic activity. Different adsorption and activation behaviors of NO on {110} and {001} facets, and different photocatalytic reaction pathways for NO removal were induced.[131] Combined above analysis, regulating the facet exposure of photocatalyst can change the microstructure properties that affect photocatalytic performance. However, research about the effect of the crystal facet for photocatalytic performance is still insufficient systematic, which needs to go further study the influence of different atom arrangement on light catalytic reaction process by more in situ characterization methods in the future.

3.2 | Electronic structure control

3.2.1 | Doping

The element doping method is one of commonly used modification methods to enhance the optoelectronic properties of Bi-based photocatalyst. Element doping mainly includes metallic element deposition and doping, nonmetallic element doping and self-doping.[133-136] (1) *Metallic element deposition and doping*. The deposition and doping of metallic elements could change the photocatalytic properties mainly in the following two aspects. First, when metal ions enter the lattice, they will change the crystallinity of the Bi-based photocatalysts or introduce defects, so as to enhance the absorption properties of light and the separation efficiency of photogenerated charges.[137-140] For instance, Regmi et al synthesized Fe-doped $BiVO_4$ with the in-gap state between the valence band and conduction band of $BiVO_4$, resulting in enhancing electron-hole separation and improving the absorption capacity of visible light. Therefore, photocatalytic degradation efficiency of IBP and inactivation of *E. coli* were improving under visible light irradiation in Figure 5A.[140] Second, surface plasmon resonance effect is generated by metallic element deposition on the semiconductor surface. The introduction of SPR can also expand the spectral response range of semiconductor and improve quantum yield. Common deposition and doping of metallic elements include Au, Ag, Bi, Fe, Ni, Co, Al, etc.[141-144] For instance, Huang et al synthesized Bi/Bi2WO6 with visible light absorption for photocatalytic decomposition of rhodamine B and 4-Chlorophenol. The SPR effect of Bi enhanced the electron-hole migration efficiency and the interfacial interaction between Bi_2WO_6 and Bi nanoparticles, and thus promoting the photocatalytic activity (Figure 5B).[144] (2) *Nonmetallic element doping*. Doping of nonmetallic elements can generate doping energy levels between the conduction band and valence band in Bi-based photocatalysts, which can not only promote light absorption to boost the utilization rate of light, but also improve the charge transmission of the Bi-based photocatalysts to promote the effective electron-hole separation, and inhibit their recombination. Common doped nonmetals include N, C, B, S, X (F, Cl, Br, I), etc.[145-147] Wu et al synthesized boron (B) doped BiOBr (B-BiOBr) nanosheets for inactivating a typical bacterium, *Escherichia coli* K-12. The B dopant would accept extra e^- from valence band of BiOBr, resulting in improving separation efficiency of charge carrier (Figure 5C).[147] (3) *Self-doping*. Self-doping is a new strategy that aims to introduce some intermediates in the synthesis process into photocatalysts so as to change energy band structure and improve the photocatalytic performance. Huang et al developed CO_3^{2-}-self-doped $Bi_2O_2CO_3$ by hydrothermal method. The light response of CO_3^{2-}-self-doped $Bi_2O_2CO_3$ was broaden from ultraviolet to visible light by continuously regulating band gap (Figure 5D). The DFT calculation results show that CO_3^{2-}-self-doping would lower the position of conduction band and generate impurity level, thus narrowing the band gap of $Bi_2O_2CO_3$.[148]

Generally, doping level includes deep level and shallow level, and the deep level can easily become the combination center of the carrier and seriously reduce the photocatalytic activity. Hence, appropriate dopants and their concentrations will importantly affect the electronic structure and improve the photocatalytic performance. The main function of appropriate doping is to enhance the photogenerated electron-hole separation efficiency and light absorption ability, thus improving the photocatalytic efficiency. Depending on the type of impurity (shallow or deep) and the properties of the valence state of the dopant (inert lattice mismatch, donor, and recipient), the following results are most likely to occur: the improved light absorption, the enhanced conductivity of charge carriers (mobility, diffusion or concentration) and the promoted photoinduced charge separation efficiency.[149,150]

3.2.2 | Heterojunction

Bi-based heterojunction photocatalysts composed of multicomponent or multiphase materials are very effective

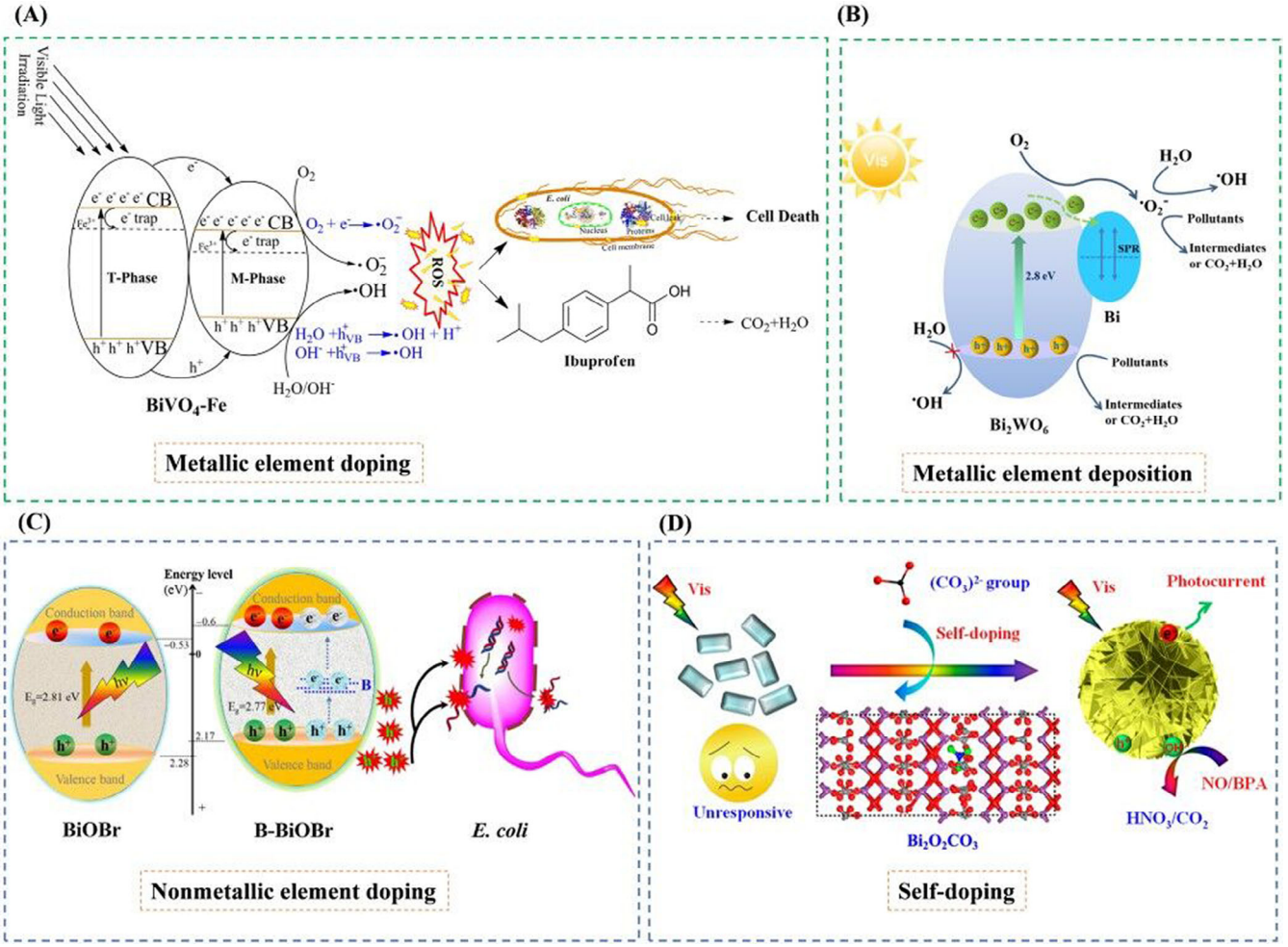

FIGURE 5 A, Schematic diagram of degradation mechanism of IBP and inactivation of *E. coli* by Fe-doped $BiVO_4$. B, The photocatalytic mechanism for organic pollutant degradation over the Bi/Bi_2WO_6 composite. C, Proposed photocatalytic bacterial inactivation enhancement of B-BiOBr nanosheets. D, CO_3^{2-}-Self-doping $Bi_2O_2CO_3$. *Source*: A, Reproduced with permission: Copyright 2017, Elsevier.[140] *Source*: B, Reproduced with permission: Copyright 2016, Elsevier.[144] *Source*: C, Reproduced with permission: Copyright 2016, Elsevier.[147] *Source*: D, Reproduced with permission: Copyright 2015, American Chemical Society[148]

strategies to design high activity photocatalytic systems. Heterojunction photocatalyst can combine heterojunction and advantages of nanomaterials, promoting the visible light absorption, charge carrier separation and charge transfer efficiency by carefully designing two or more different materials or phase of the semiconductor materials. Therefore, this strategy has great potential application prospects in photocatalysis.[151-154] Generally, the semiconductor-semiconductor heterojunction could be classified as straddle gap (type I), staggered gap (type II), and broken gap (type III) according to the band arrangement in Figure 6A. Among those heterojunctions, type II heterojunction has been extensively studied owing to its excellent photogenerated electron-hole separation.[155,156] According to the type of contact semiconductor and the mechanism of charge transfer and separation between them, type II heterojunction mainly includes p-n, n-n (p-p) and Z-scheme heterojunction (Figure 6B). By constructing heterojunction, the electronic structure of photocatalyst can be regulated to promote absorbing ability of light and enhance the photogenerated charge separation and migration. (1) *The p-n heterojunction*. By the built-in electric field of interface, photogenerated holes in n-type semiconductor are migrated to p-type semiconductor while the photogenerated electrons are migrated from p-type semiconductor to n-type semiconductor, thus promoting the effective separation and life extension of photoinduced electron-hole pairs (Figure 6B).[157-160] He et al prepared a $BiOCl/BiVO_4$ p-n heterojunction photocatalyst via hydrothermal method, which owns visible-light absorption and efficient charge separation and transfer, promoting the removal of methyl orange (MO).[161] Zou et al synthesized the flower-like $BiPO_4/BiOBr$ p-n heterojunction composites, which enhanced the separation of photoinduced electron-hole pairs and thus showed higher photocatalytic degradation

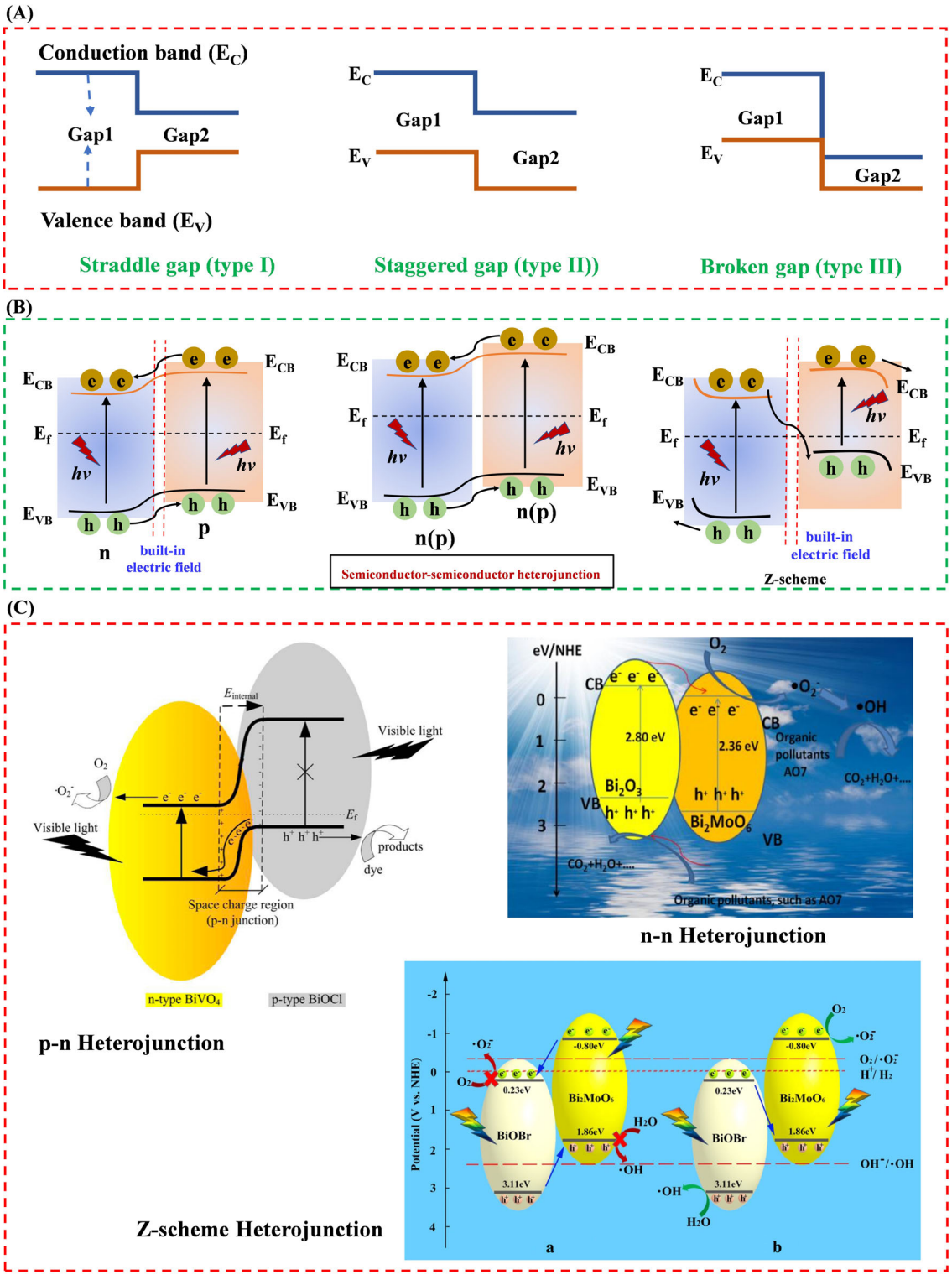

FIGURE 6 A, Energy band diagram of three semiconductor heterojunctions. B, Band diagrams of common p-n heterostructure, p-p (n-n) heterostructure and Z-scheme heterojunction. C, The p-n heterojunction BiOCl/$BiVO_4$ photocatalyst, Bi_2O_3/Bi_2MoO_6 heterojunction photocatalysts with n-n type heterojunction structure and BiOBr-Bi_2MoO_6 with Z-scheme heterojunction structure. *Source*: A, Reproduced with permission: Copyright 2012, Royal Society of Chemistry.[155] *Source*: B, Reproduced with permission: Copyright 2014, Elsevier.[81] Copyright 2014, Elsevier.[171] *Source*: C, Reproduced with permission: Copyright 2014, American Chemical Society.[161] Copyright 2018, Elsevier.[163] Copyright 2017, Elsevier[168]

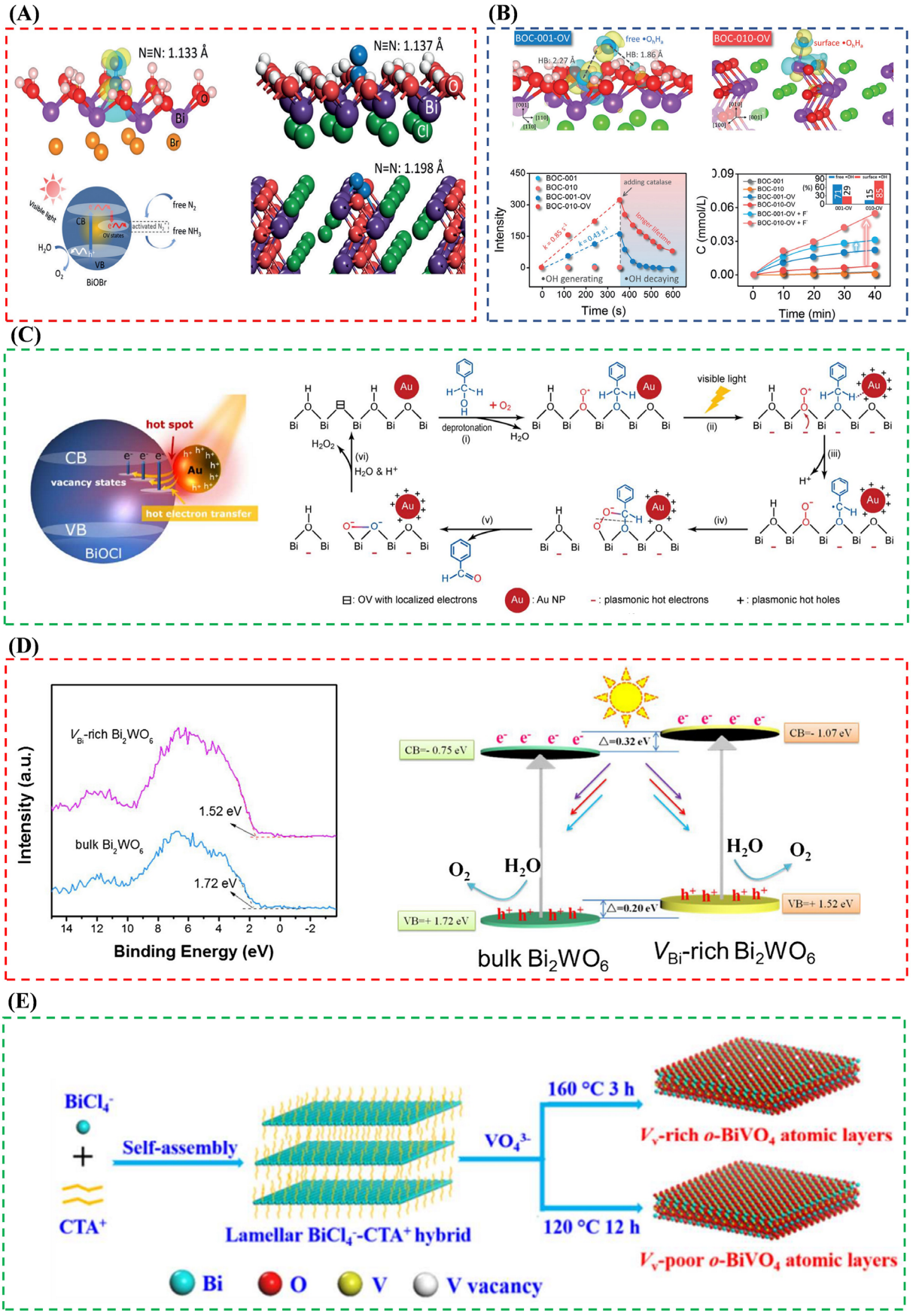

FIGURE 7 Legend on next page.

efficiency of gaseous 1,2-dichlorobenzene (*o*-DCB) under visible light.[162] (2) *The p-p (n-n) heterojunction*. The potential difference between the two semiconductors drives the photogenerated electron-hole separation without built-in electric field (Figure 6B). Yi et al prepared Bi_2O_3/Bi_2MoO_6 heterojunction photocatalysts with n-n type heterojunction structure, which promoted the visible-light response and enhanced photogenerated charge separation, and thus the degrading efficiency of acid orange 7 (AO7) was improved.[163] (3) *The Z-scheme heterojunction*. The Z-scheme heterojunction is a special kind of heterojunction, which is different from p-n heterojunction. For Z-scheme heterojunctions, the direction of electron flow is transferred from conduction band of semiconductors with positive conduction band position to valence band of another semiconductor with negative conduction band position. The electron transport process is shown in Figure 6B, which would decrease photogenerated electron-hole recombination on semiconductors with negative conduction bands and enable photogenerated electrons to be used for reduction.[164-167] Wang et al fabricated a BiOBr-Bi_2MoO_6 photocatalyst with Z-scheme heterojunction, which greatly improved photocatalytic performance attributing to the efficiently transferred of carriers in sandwiched layers.[168]

By constructing above heterojunctions, Bi-based photocatalysts can improve absorption of visible light and obtain efficient electron-hole separation, thus improving photocatalytic performance. In addition to the formation of above traditional heterojunctions, the zonal arrangement of different crystalline surfaces from the same material can form surface heterojunctions, which can greatly enhance charge separation.[169] In recent years, the surface heterojunction as a new concept has brought about widespread attention. The surface heterojunction of Bi-based photocatalysts has been developed in $BiVO_4$.[170] Therefore, it will be a potential opportunity to develop and study more Bi based surface heterojunction photocatalysts in the future.

3.2.3 | Defect engineering

The surface defects can determine the electronic structure and chemical properties of Bi-based photocatalyst, including light absorption, conductivity, carrier diffusion dynamics, thermoelectric power.[171-174] The defects are mainly divided into deep defects and surface defects inside the crystal. In the crystal, photogenic electrons and holes are easy to recombine in the deep defect, reducing the photocatalyst activity, so the formation of deep defect should be avoided as far as possible in the synthesis process. Defects in the surface of the crystal could also trap charges, but they are released quickly, and the brief capture could facilitate the electron-hole separation, enhancing photocatalyst performance. An appropriate amount of surface defects will has important effects on the energy band structure and excitation process of Bi-based photocatalyst, and the surface defects will form partial overlap between the shallow energy level and the state density of the valence band near the top of the valence band in the forbidden zone, thus widening the width of the valence band and reducing the forbidden band width. In Bi-based photocatalyst, oxygen defect is the most common and widely studied anionic defect as its formation energy is relatively low. Localized states induced by oxygen vacancy (OV) can extend the light response range and effectively capture charge carriers, thus enhancing the mechanism of influence on dynamics, energetics and further catalytic processes. The oxygen defects with abundant local electrons can enhance the interaction between oxygen and oxide surface and promote charge transfer at the interface.[175-178]

Recently, Zhang et al found that defects on the surface of BiOBr will enhance the N_2 adsorption and activation to achieve efficient photocatalytic nitrogen fixation (Figure 7A).[179] But the effect of OVs on the thermodynamics of photocatalytic nitrogen fixation is not clear at present. Zhang et al then used BiOCl-OV as a model catalyst to continue to study the kinetics and thermodynamics of nitrogen fixation, and to define the control steps of the reaction. As shown in Figure 7B, H_2O_2 on BiOCl-001-OV can dissociate spontaneously and one of the —OH groups is fixed at the defect and the other —OH group is far away from the surface. Similar H_2O_2 dissociation took place on the BiOCl-010-OV surface while the dissociated —OH group tended to adsorb on the Bi atom close to OV to form·OH.[180] As shown in Figure 7C, a new plasma photocatalyst was formed by depositing precious metal Au on {001} of oxygen-deficient BiOCl. The results show that oxygen defect can capture hot electrons while the energy is insufficient to directly go

FIGURE 7 A, Defects enhance the N_2 adsorption and activation to achieve photocatalytic nitrogen fixation. B, The dissociation of H_2O_2 on different crystal surfaces of defective BiOCl. C, The morphology of Au-BiOCl-001-OV catalyst and the effect of defects on the thermal electron transport. D, XPS valence spectra of the obtained samples and schematic band structure of bulk Bi_2WO_6 and V_{Bi}-rich Bi_2WO_6. E, Scheme of synthesizing the V_v-rich and V_v-poor o-$BiVO_4$ atomic layers. *Source*: A, Reproduced with permission: Copyright 2015, American Chemical Society.[179] *Source*: B, Reproduced with permission: Copyright 2017, American Chemical Society.[180] *Source*: C, Reproduced with permission: Copyright 2017, American Chemical Society.[181] *Source*: D, Reproduced with permission: Copyright 2018, Elsevier.[182] *Source*: E, Reproduced with permission: Copyright 2017, American Chemical Society[183]

through the Schottky barrier. Coupled with thermal holes with mild oxidation ability and OVs with enhanced oxygen adsorption, Au-BiOCl-001-OV has a great prospect of selective alcohol oxidation.[181]

Compared with widely studied oxygen vacancies, there are few reports about the photocatalyst with mental vacancies and the influence of metal defects on the photocatalytic properties. Di et al reported a single unit cell ultrathin Bi_2WO_6 nanosheets with bismuth vacancies via a template-directed strategy. The bismuth vacancies increased charge carrier concentration and electronic conductivity by forming a new defect level to improve density of states at the valence band maximum. Additionally, the bismuth vacancy structure can enhance adsorption and activation of H_2O molecule, favoring the water oxidation reactions (Figure 7D). Therefore, the Bi_2WO_6 with rich bismuth vacancies showed an enhanced photocatalytic oxygen evolution activity than Bi_2WO_6.[182] Xie et al reported a single-unit-cell o-$BiVO_4$ layers with vanadium vacancy as defect level in Figure 7E, and the hole concentration of o-$BiVO_4$ is higher near Fermi level. Therefore, the light absorption and electronic conductivity could be enhanced.[183]

Although the research of defective nanomaterials in photocatalysis has become more and more intensive in recent years, the mechanism of defects in photocatalysis is still unclear. On the one hand, defects may be the photogenerated carrier recombination center, playing a negative role. On the other hand, defects may promote the adsorption and activation of substrates, participate in photocatalytic reaction and play a positive role. To study the mechanism of defects in photocatalysis, not only advanced characterization methods, such as EXAFS, XPS and EPR, but also rigorous experimental design and profound theoretical analysis and calculation are needed.

4 | REACTION MECHANISMS OF BISMUTH-BASED PHOTOCATALYTIC MATERIALS

4.1 | Bi-based semiconductor photocatalytic mechanism

Most Bi-based photocatalysts belong to semiconductor and thus most of them conform to the mechanism of semiconductor photocatalysis.[81,152,184] Based on the solid energy band theory, energy band structure of solid materials can be divided into three parts: valence band, forbidden band and conduction band. Figure 8A shows a schematic of a photoexcited semiconductor. In photocatalytic reaction, the generation, separation and redox of photoinduced electron-hole pairs determine the efficiency of photocatalytic reaction and are influenced by many factors. (1) *The formation of photogenerated electron-hole pairs*. Electrons in the highest valence band are excited by a certain energy of light ($h\nu \geq Eg$) to jump to the lowest unoccupied conduction band, forming a highly reductive electron (e^-) while leaving a strongly oxidized hole (h^+) in valence band, producing electron-hole pairs. This process is mainly affected by the properties of the semiconductor itself, and the size of Eg determines the spectral response range. In order to fully utilize solar light source, developing photocatalysts with visible light response is an important development direction in the future. (2) *Photogenerated electron-hole pair separation and migration*. The electron-hole pair migrated to the photocatalyst surface to participate in the redox reaction. During the migration, a large number of photogenerated electrons and holes would recombine while only a small number of them would take part in the reaction. The recombination reaction between photogenerated electrons and holes releases energy in the form of light or heat, which reduces the quantum efficiency of photocatalytic materials and is extremely unfavorable to the photocatalytic performance. Therefore, the occurrence of this process should be avoided as far as possible. (3) *Redox reaction*. These photogenerated electron-hole pairs with strong redox characteristics migrate and diffuse to the surface of the photocatalyst to apply in removal of nitrogen oxides, degrade organic matter, hydrogen production and CO_2 reduction through redox reactions.

4.2 | Bi-metal based plasma photocatalytic mechanism

Previous studies have shown that bismuth could transform from semimetallic to semiconductor properties with the decrease of its size, which may lead to the transition from plasma resonance mechanism to semiconductor mechanism in photocatalytic mechanism. Figure 8B,C are deep level transitions of semimetallic bismuth and plasmonic resonance photocatalytic mechanism of bismuth.[61,63] With the light absorption and SPR excitation of bismuth nanoparticles, plasma decay may occur through three mechanisms.[185-187] (a) Elastic emission of photons that the adsorbed molecules can get energy by absorbing photons from the strongly reradiated photon flux of the plasma nanostructure. (b) The photon energy is converted to single electron-hole pair excitations, named Nonradiative Landau damping. (c) The interaction between excited surface plasmons and adsorbates, inducing directly injecting electron into the adsorbates.[44]

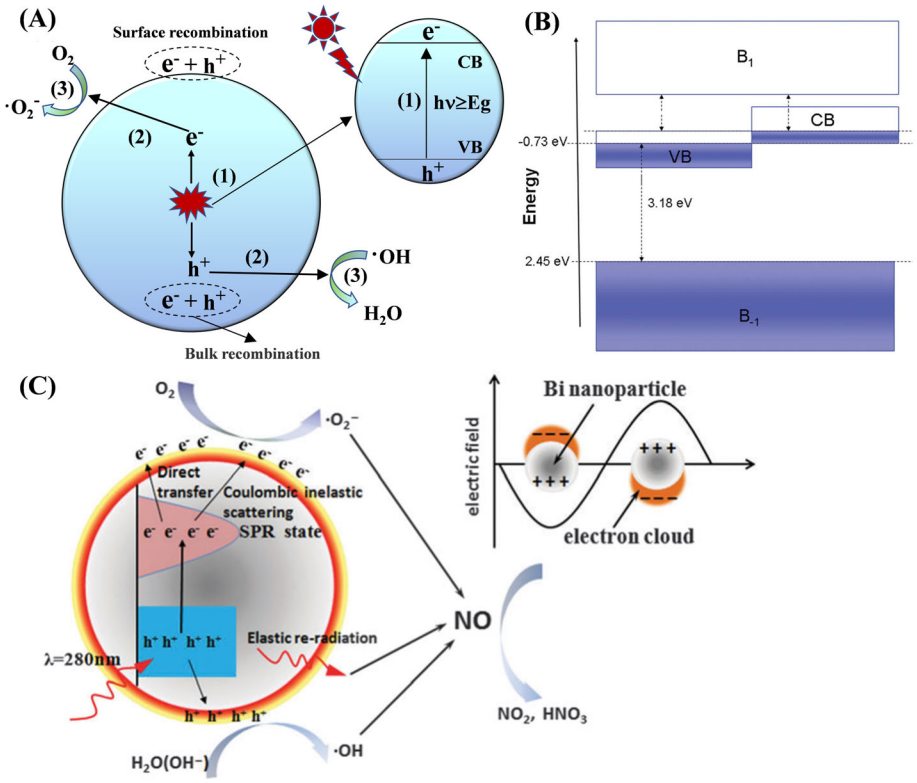

FIGURE 8 A, Photoexcited semiconductor mechanism. B, The deep level transition of semimetallic bismuth. C, The mechanism of plasma resonance photocatalysis of bismuth. *Source*: B, Reproduced with permission: Copyright 2014, Royal Society of Chemistry.[63] *Source*: C, Reproduced with permission: Copyright 2014, Royal Society of Chemistry[61]

In addition, although theoretical calculations show that the properties of bismuth will change from semimetallic to semiconductive when the particle size of bismuth is less than 70 nm, the critical size of bismuth transformation is different and closely related to its morphology in the actual experimental process. At the same time, the photocatalytic performance of bismuth as a plasmonic photocatalytic material is excellent. The plasmon resonance effect varies with the size and morphology. Therefore, it is very important to explore the effects of the light absorption for photocatalytic properties of bismuth with different sizes.

4.3 | Bi-metal based semiconductor/plasma synergistic mechanism

Recently, Dong et al found that integration of Bi plasmonic nanoparticles into Bi-based semiconductor photocatalyst can be utilized as an attractive method to synthesize visible-light-induced plasmonic photocatalysts, which are considered as one of the most promising alternatives to traditional photocatalyst. Compared with noble metals such as Au or Ag, non-noble metals such as Bi own significant strengths of easy availability, low cost and facile synthesis. More importantly, the new catalytic reaction mechanism was proposed through systematic research and understanding of semiconductor/plasmonic Bi co-catalyst system.[143,188-192] As shown in Figure 9A, Dong et al[143] developed in situ deposited Bi co-catalyst on $(BiO)_2CO_3$ microspheres and reported the photocatalytic mechanism of NO oxidation. The interface transfer of electrons reduces the electron-hole recombination (I). First, the SPR effect of Bi propel more absorption of visible light and enhances the surface electron excitation of Bi particles. Second, the photoinduced electrons in Bi would transfer to $(BiO)_2CO_3$ owing to higher Fermi level of metal Bi than $(BiO)_2CO_3$ conduction band. Third, once electrons are released, Bi would accept electrons from $(BiO)_2CO_3$ valence band to return to its primal state. Moreover, SPR mediated local electromagnetic field of Bi (II) also promotes electron-hole generation and separation in $(BiO)_2CO_3$ (Figure 9A). Then, the separated electrons and holes would participate in redox reaction. Similar experimental results and mechanisms were further proposed in Bi-Bi_2MoO_6 (Figure 9B). But it is noted that the metal Bi Fermi level is lower that the Bi_2MoO_6 conduction band,[190] which indicates an opposite electron transport pathway compared with Bi-$(BiO)_2CO_3$ (Figure 9A).

Furthermore, Dong et al in situ constructed Bi metal@defective BiOBr to remove NO in air.[192] The charge transmission path and photocatalytic mechanism shown in Figure 9C,D. The DFT calculations about charge

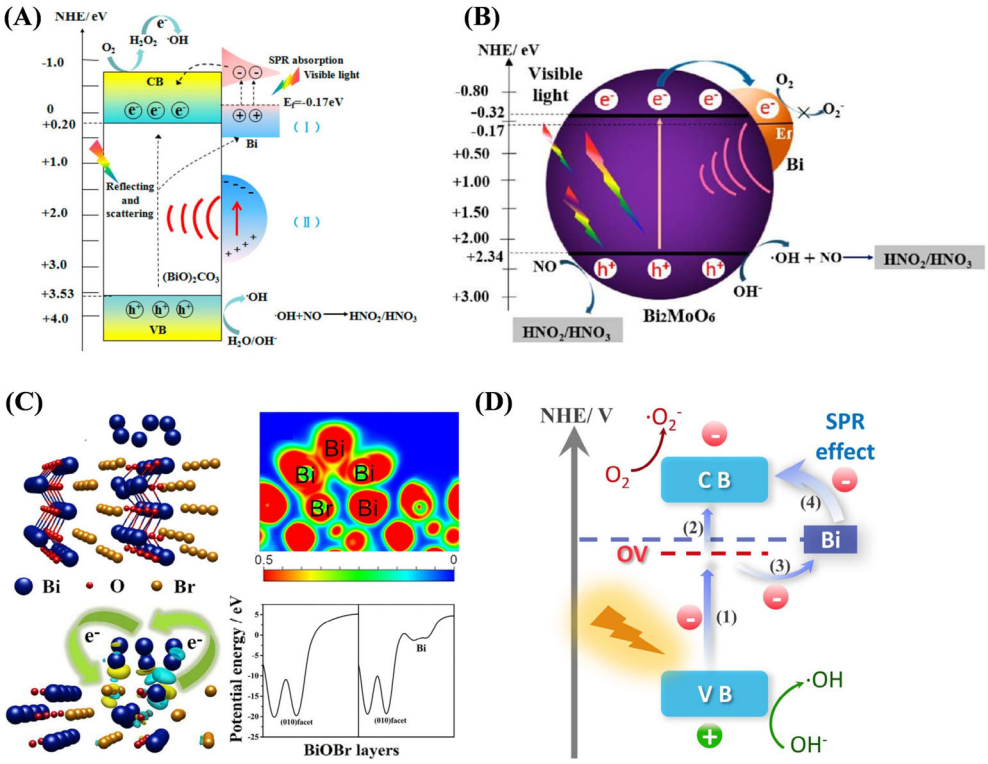

FIGURE 9 Photocatalytic mechanism scheme: A, Bi/BOC, B, Bi/Bi_2MoO_6, and C, The DFT calculates the charge transfer on Bi/BiOBr. D, The charge transferred mechanism of Bi metal@defective BiOBr. *Source*: A, Reproduced with permission: Copyright 2014, American Chemical Society.[143] *Source*: B, Reproduced with permission: Copyright 2016, American Chemical Society.[190] *Source*: C, D, Reproduced with permission: Copyright 2018, Elsevier[192]

transfer on Bi/BiOBr indicate Bi metal would affect separation and transmission of photogenerated charges on BiOBr. The synergistic effects of oxygen vacancies and Bi metal would form a novel charge transferred channel, which can improve the separation efficiency of electron-hole pairs and also facilitate the production of reactive oxygen species (Figure 9D). Therefore, the Bi metal@defective BiOBr exhibited greatly enhanced photocatalytic performance. A similar mechanism will be found in Bi/BiOCl with oxygen vacancies[191] and $Bi/Bi_2O_2CO_3$ with oxygen vacancies.[193]

5 | APPLICATIONS OF BISMUTH-BASED PHOTOCATALYTIC MATERIALS

At present, the Bi based photocatalysts have been widely used in the fields of energy conversion and environmental remediation. The main environmental areas are photocatalytic degradation of pollutants, including sewage treatment, air purification, deodorization and sterilization. The energy application focused on photocatalytic hydrogen production, CO_2 reduction to small molecule organic matter (such as methane, methanol, etc.) and N_2 fixation.[39,44,81,194-196] In this part, we summarized the application status of Bi-based photocatalysts in recent years.

5.1 | Environmental photocatalysis

5.1.1 | Photocatalytic purification of typical atmospheric pollutants

With the rapid development of urbanization and economy, plentiful pollutants were discharged by human activities and have caused serious atmospheric pollution. The primary pollutants are discharged into the atmosphere including sulfur compounds, nitrogen compounds, organic pollutants and particulate matter. Many primary gaseous pollutants can produce many secondary pollutants (such as secondary fine particles, ozone, etc.) through complex physical and chemical processes in the atmosphere.[197-199] The semiconductor photocatalytic materials could be used in urban construction, road laying, building decoration materials and air cleaners, the typical air pollutants nitrogen oxides, carbon monoxide, VOCs and other substances can be directly converted into harmless substances under the light.

Recently, Dong et al designed a variety of Bi-based semiconductor photocatalysts for the purification of nitrogen oxides (NO_x) and made many important advances. The introduction of oxygen vacancies (OV) in $Bi_2O_2CO_3$ can broaden range of light absorption, enhance separation efficiency of charge, and improve activation of the reactants (Figure 10A).[200] Therefore, the photocatalytic NO removal efficiency was increased significantly. However,

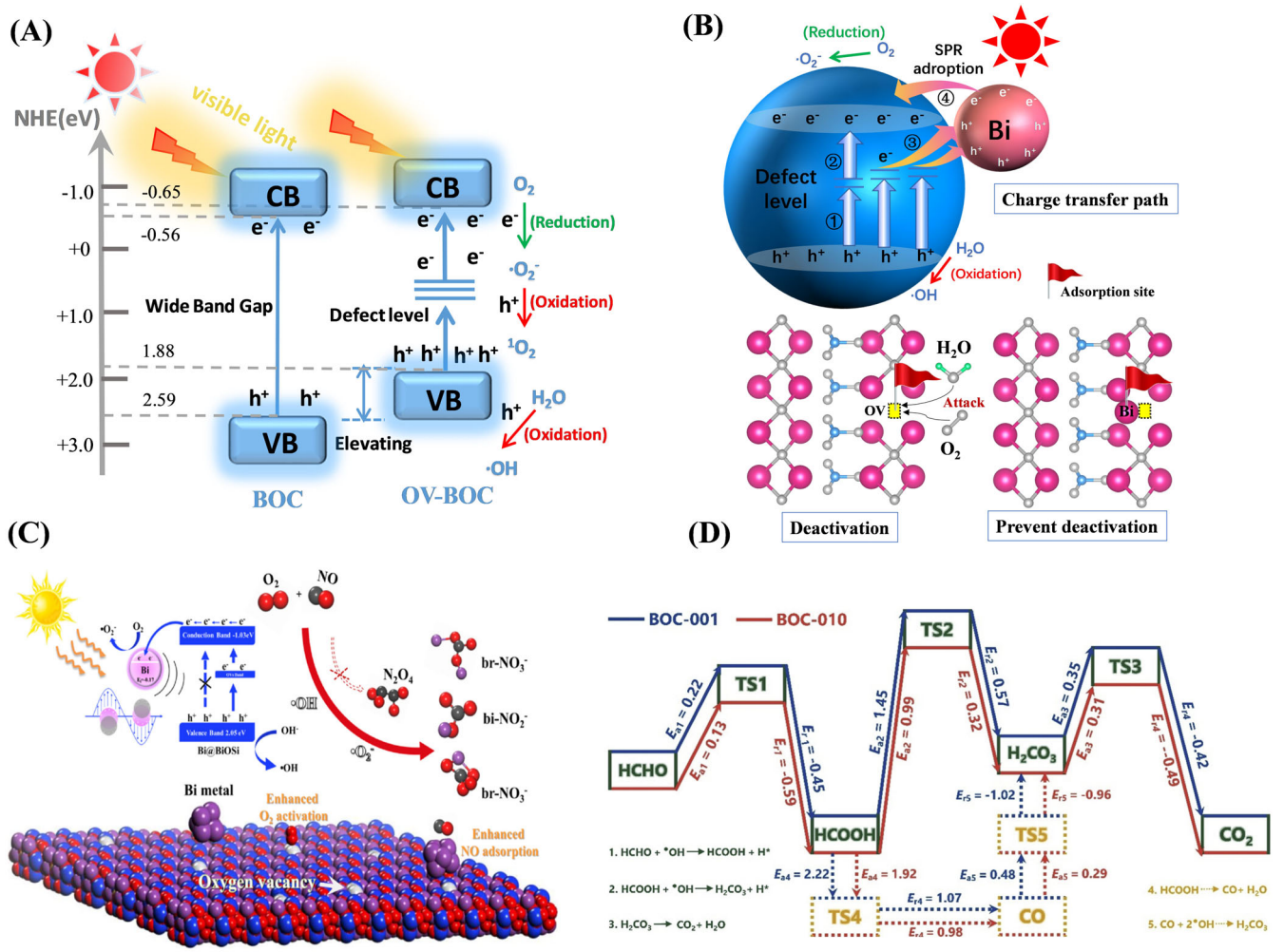

FIGURE 10 A, Schematic diagram of reactive oxygen generation and band structure on OV-BOC. B, Schematic illustration of charge transfer path and active site in $Bi_2O_2CO_3$. C, Scheme of photocatalytic NO removal on $Bi/Bi_2O_2SiO_3$. D, Calculated activation energies (E_a) and reaction energies (E_r) for the primary reaction pathways in HCHO degradation. *Source*: A, Reproduced with permission: Copyright 2019, Elsevier.[200] *Source*: B, Reproduced with permission: Copyright 2020, Elsevier.[193] *Source*: C, Reproduced with permission: Copyright 2019, Elsevier.[201] *Source*: D, Reproduced with permission: Copyright 2020, Elsevier[202]

they also found that the surface oxygen vacancies were unstable over a long period of reaction time. Further, Dong et al deposited the Bi metal on $Bi_2O_2CO_3$ with oxygen vacancies. It was found that the synergistic effect of Bi and OVs would highly facilitate the separation of photogenerated electron-hole pairs to product abundant active radicals. Additionally, the Bi nanoparticles could prevent from O_2 and H_2O molecules filling into oxygen vacancies, which improve the stability of oxygen vacancies (Figure 10B).[193] In addition, a visible light catalyst ($Bi/Bi_2O_2SiO_3$) with SPR characteristics indicated the formation of a unique electron transfer channel at interface of $Bi/Bi_2O_2SiO_3$ in Figure 10C, which exhibited enhanced performance for photocatalytic atmospheric NO removal at ppb level.[201] In addition, Dong et al revealed the correlation between BiOCl and photocatalytic purification of formaldehyde (HCHO) by regulating different exposed crystal surfaces. Combined with in situ FTIR and density functional theory (DFT) calculation results, the formic acid (HCOOH) was found to be the most important and stable intermediate product in photocatalytic degradation of formaldehyde, and thus oxidation of formic acid (HCOOH) is the determining step of the overall degradation rate of formaldehyde, as shown in Figure 10D.[202]

5.1.2 | Photocatalytic degradation of liquid phase pollutants

Compared with the traditional water pollution treatment method, the photocatalytic method is environmentally friendly and has no secondary pollution. In addition to common dyes such as methyl orange (MO), rhodamine B (RhB) and methylene blue (MB), other colorless pollutants such as

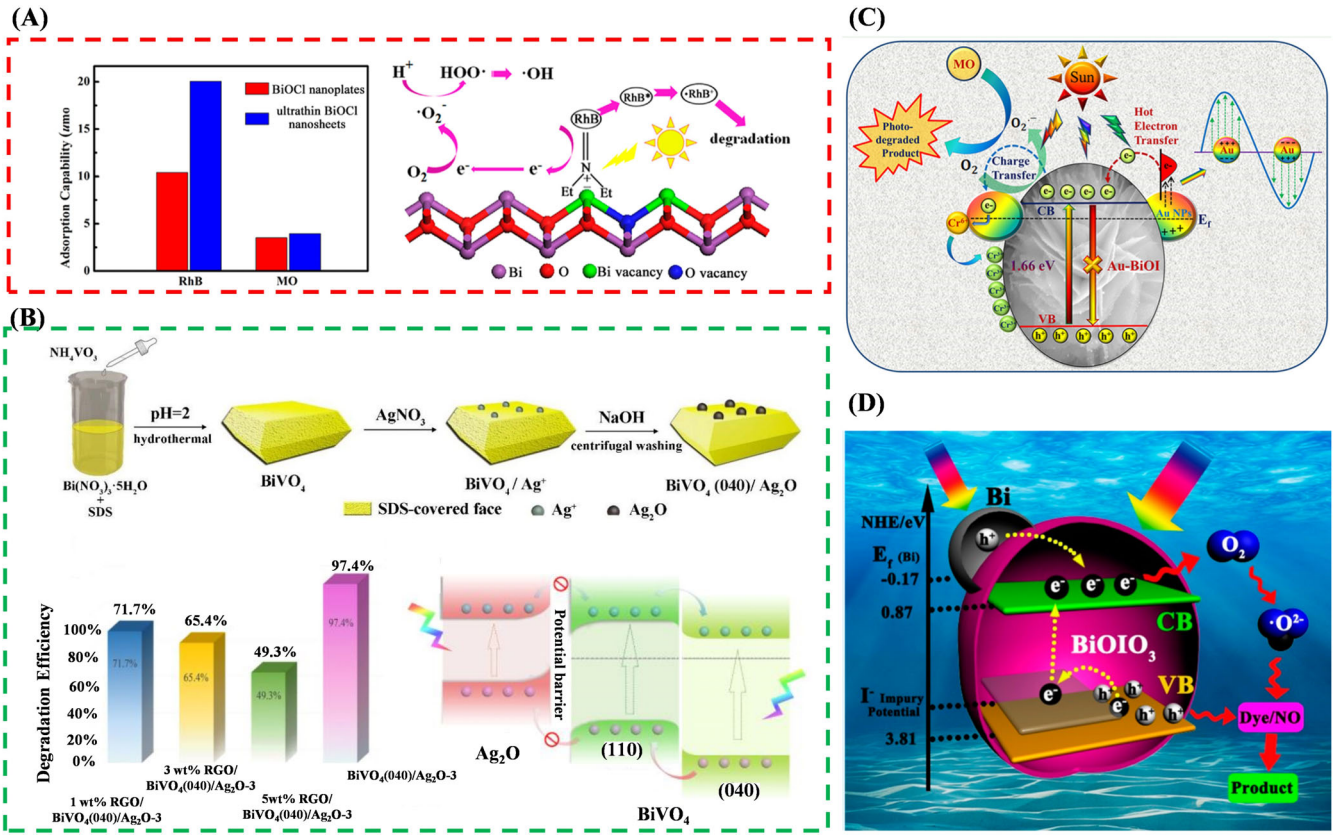

FIGURE 11 A, The RhB and MO adsorption on BiOCl photocatalyst and schematic diagram of photosensitization process. B, The synthesis of $BiVO_4$ (040)/Ag_2O and MB solution photodegradation. C, The mechanism for photocatalytic methyl orange and Cr(VI) detoxification on Au-BiOI. D, The possible photocatalytic mechanism and charge separation in $BiOIO_3$. *Source*: A, Reproduced with permission: Copyright 2013, American Chemical Society.[88] *Source*: B, Reproduced with permission: Copyright 2019, Elsevier.[206] *Source*: C, Reproduced with permission: Copyright 2020, American Chemical Society.[207] *Source*: D, Reproduced with permission: Copyright 2015, American Chemical Society[208]

bisphenol A(BPA), phenol, or various antibiotics and pesticides can be also degraded. In addition, photocatalysis can also reduce toxic heavy metal ions (such as Cr^{6+}) to low-cost ions in water bodies, which can weaken their toxicity. Photocatalytic elimination of environmental pollutants mainly involves the oxidation of organic pollutants by active ROS such as $\bullet O_2^-$, •OOH, •OH, etc and the final goal of eliminating organic pollutants is achieved through a series of complex reactions.[203-205] Xie et al designed and synthesized two-dimensional ultra-thin BiOCl nanostructure with defect state, thus realizing the high photocatalytic degradation efficiency of rhodamine B (RhB) and revealing the structure-performance relationship, as shown in Figure 11A.[88] In addition, Wang et al selectively deposit Ag_2O nanoparticles onto $BiVO_4$ (040) facet. The $BiVO_4$(040)/Ag_2O heterostructures owns the excellent capability in light absorption and the efficient charge separation, which enhanced the photocatalytic methylene blue (MB) degradation activity and O_2 evolution in Figure 11B,[206] Chatterjee et al synthesized a 3D flower-like BiOI microspheres with plasmonic Au nanoparticle decoration, which shows an outstanding photocatalytic detoxification for organic (methyl orange) as well as inorganic (hexavalent chromium) water pollutants (Figure 11C).[207] Yu et al simultaneously achieved I^- doping and plasmonic Bi metal deposition in $BiOIO_3$. And Bi/I^- co-decorated $BiOIO_3$ exhibits widely strong photo-oxidizing performance toward multiple pharmaceutical and industrial contaminant decomposition, including tetracycline hydrochloride, dye model Rhodamine (RhB), bisphenol A (BPA), 2,4-Dichlorophenol (2,4-DCP), phenol (Figure 11D).[208] For photocatalytic removal of dyes in water, much attention should be paid to photosensitization effect of dyes themselves under visible light irradiation. Typically, colorless pollutants should be chosen as target pollutants.

5.1.3 | Photocatalytic disinfection and sterilization

Bacteria and viruses can be treated with a variety of different technologies, including heat, ultraviolet radiation,

antibiotics, and chemical oxidation. However, antibiotics are selective and slow to kill bacteria and viruses. Chemical oxidation, while effective in inactivating bacteria and most viruses, produces unwanted byproducts. Therefore, clean and effective solar photocatalytic sterilization and disinfection has gradually attracted researchers' attention. Xiang et al prepared p-n heterostructure photocatalyst Bi_2WO_6/BiOI by chemical etching, which exhibited great properties for methyl blue (MB) degradation in visible light and the sterilization of *Pseudomonas aeruginosa*, *E. coli* and aureus.[209] The photocatalytic technology has also been applied in disinfection and sterilization of air, showing advantages in comparison with traditional technology.

5.1.4 | Summary discussion

Based on the above analysis, Bi-based semiconductor photocatalyst has good application potential in pollutant purification and sterilization. For photocatalytic purification of pollutants or sterilization, semiconductor photocatalysts are usually required to have sufficient oxidation capacity. The semiconductor would be excited via absorbing a certain amount of light absorption to generate electrons and holes, which are then separated and migrated to the surface to react with the adsorbents to form active free radicals and participate in the reaction on the catalyst surface, or the holes directly participate in the oxidation reaction. Therefore, sufficient free radicals and appropriate semiconductor valence band potential after electron and hole separation are critical for photocatalytic purification of pollutants and sterilization. In Section 3, the structural control strategy has been given. The valence band position of bismuth—based semiconductor can be effectively regulated by elemental doping. The construction of heterojunctions and defects can regulate the separation and transfer of photogenerated electrons and holes. In addition, the adsorption and activation of reactants in photocatalytic reactions are also the key factors determining the performance of photocatalytic reactions, and the regulation of morphology, size and crystal surface exposure can effectively realize the regulation of adsorption and activation performance. Appropriate methods can be adopted to design and synthesize new Bi-based semiconductor catalysts with appropriate electronic band structures.

5.2 | Energy photocatalysis

5.2.1 | Photocatalytic reduction of CO_2

Since the late 19th century, the concentration of atmospheric CO_2 has increased from 280 ppm to 408 ppm today. In this context, the exploration of effective reduction of CO_2 concentration in the atmosphere has become a key research direction of governments and scientists.[210-212] Among the available strategies, the photochemical reduction of CO_2 and its conversion into a hydrocarbon fuel for humans is particularly attractive. Because this method can be carried out under normal temperature and pressure, the energy required can be directly or indirectly provided by renewable energy of solar energy, truly realizing the recycling of carbon. Therefore, the use of photocatalysis to eliminate excess CO_2 in the environment while obtaining clean energy is of great significance to the environment and energy.[195,213] However, photocatalytic CO_2 reduction is much difficult due to the following reasons: (a) The O═C═O fracture of CO_2 requires high activation energy. (b) CO_2 reduction to methanol and methane is a 6-electron and 8-electron transfer process, respectively. Compared with the 4-electron transfer process of water decomposition, CO_2 reduction is much more difficult. (c) The reduction of CO_2 to methanol and other fuels involves not only the reduction process of CO_2 itself, but also complex multi-step intermediate processes such as proton transfer and hydroxylation. (d) Reduction of CO_2 in the liquid phase system is usually accompanied by the competitive reaction (proton reduction). In addition, CO_2 reduction often has a variety of products, and the selectivity of catalyst is particularly important. Therefore, the design of excellent reduction catalyst is particularly important. In recent 10 years, Bi-based photocatalyst has been considered as excellent new kind of photocatalytic material for CO_2 reduction due to its good bandgap characteristics and unique electronic structure.[39,48,196,214,215]

Recently, it was found that the vacancy defects in bismuth-based photocatalysts could facilitate CO_2 adsorption and activation to enhance the efficiency of bismuth-based photocatalysts in CO_2 reduction in Figure 12A.[216] The $Bi_4O_5Br_2$ photocatalyst was synthesized by molecular precursor method to enhance photocatalytic activity of CO_2 reduction in Figure 12B. The research results indicate that bismuth-rich and ultrathin structures could generate CH_4 and CO with high selectivity, respectively.[217] Figure 12C shows the properties of photocatalytic CO_2 reduction induced by the regulation of different exposed crystal faces of BiOI.[218]

5.2.2 | Photocatalytic decomposition of water to produce hydrogen

At present, energy consumed by human life mainly depends on the limited and unsustainable storage of fossil fuels. Therefore, developing sustainable clean energy is of great significance. The main sources of hydrogen

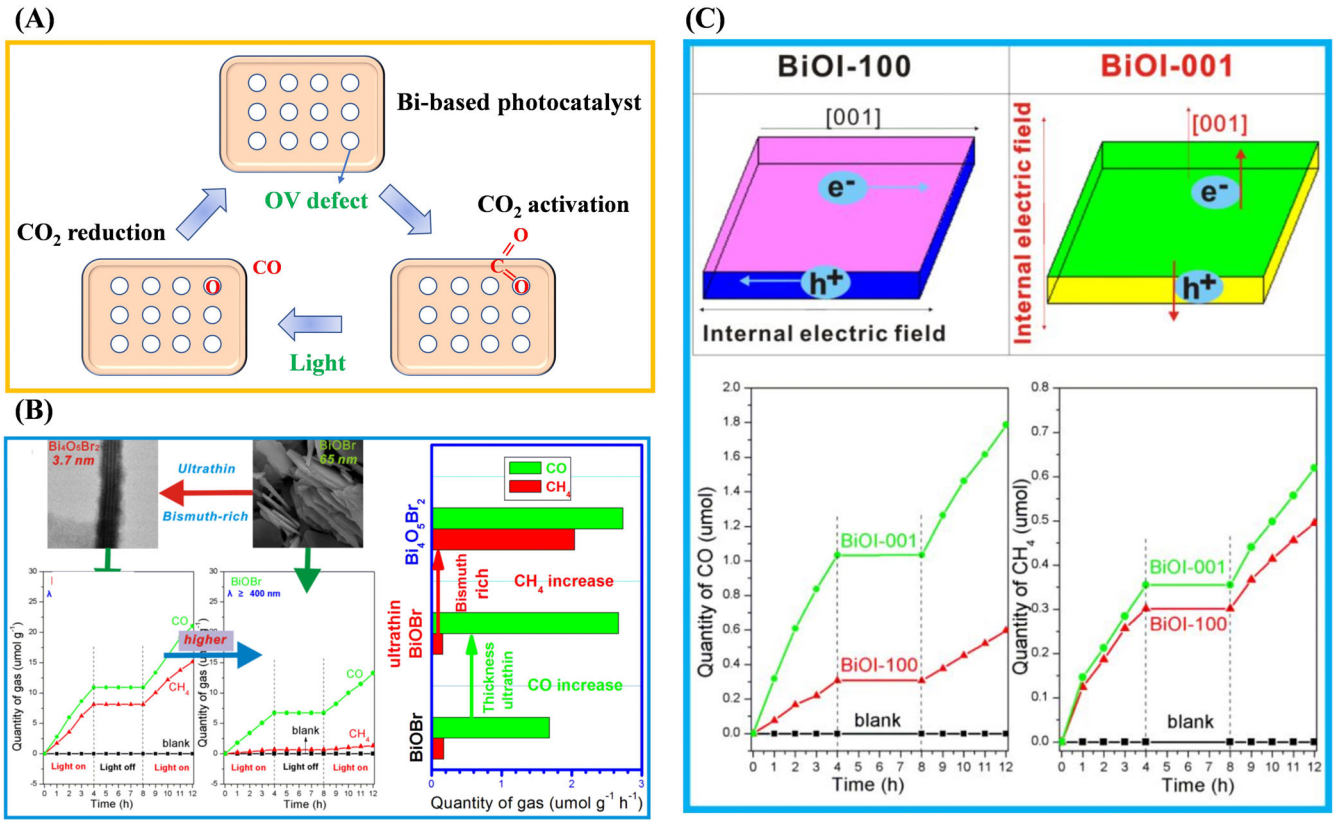

FIGURE 12 A, The photocatalytic CO_2 reduction processes on Bi-based photocatalysts. B, The effect of bismuth-rich and ultrathin strategies for photocatalytic CO_2 reduction on BiOBr. C, The photocatalytic CO_2 reduction on BiOI nanosheets with exposed different facets. *Source*: B, Reproduced with permission: Copyright 2016, Elsevier.[217] *Source*: C, Reproduced with permission: Copyright 2016, Elsevier[218]

energy are: electrolysis water to produce hydrogen, solar energy to decompose water, fossil energy reforming to produce hydrogen and so on. Among them, the solar energy decomposition of water to hydrogen has many advantages, which is also regarded as an ideal method for hydrogen production.[39,48,196,214,215] The decomposition of water is reaction of increasing the Gibbs free energy, and energy required for that reaction is obtained from sunlight. Currently, there are still challenges for photocatalysts to realize efficient photocatalytic decomposition of water: (a) Quantum efficiency is low in visible light; (b) Photocatalysts with visible light response, such as sulfides and nitrogen oxides, have poor photostability, such as sulfides are often inactivated by photocorrosion; (c) O_2 desorption from the surface of photocatalyst is very difficult, so it is often necessary to add hole (h^+) sacrificial agent in the system to promote the production of H_2. Besides, O_2 production is a 4-electron process ($2H_2O \rightarrow 4H^+ + O_2 + 4e^-$), which is relatively difficult in kinetics and requires high overpotential. And thus it is often the speed-controlled step of photocatalytic reaction; (d) In the actual photocatalytic reaction, the 2-electron process ($2H_2O \rightarrow H_2O_2 + 2H^+ + 2e^-$, competitive reaction) produces the intermediate product H_2O_2 which is difficult to remove from the surface of the catalyst, and the catalyst would get deactivated due to the occupation of the surface active site; (e) Some catalysts with high performance, such as precious metals (Pt, Pd, Au, etc., are often co-catalysts), photocatalysts containing Cd, Pb and other elements (such as CdS), are often expensive and not environmentally friendly.[219,220]

From the perspective of catalytic reaction kinetics, one possible method to improve the performance of photocatalytic water decomposition is designing photocatalyst to change the photocatalytic reaction kinetics processes. Zhang et al reported that the BiOCl with surface/subsurface defects could achieve water splitting without any co-catalysts or sacrificial agent under light irradiation. The DFT results indicate surface oxygen vacancies can effectively adsorb and dissociate H_2O molecules, which can improve water-splitting performance.[221] Zhang et al combined with experiment and DFT to study the role of oxygen vacancies in photocatalytic water oxidation on CeO_2, which indicates that the oxygen vacancies can lower the barrier energy for O-O bond formation and restrain the reverse reaction of O and H, thus the O_2 generation kinetics on oxygen-defective CeO_2 are improved significantly (Figure 13A).[222] Sun et al synthesized the quantum-sized

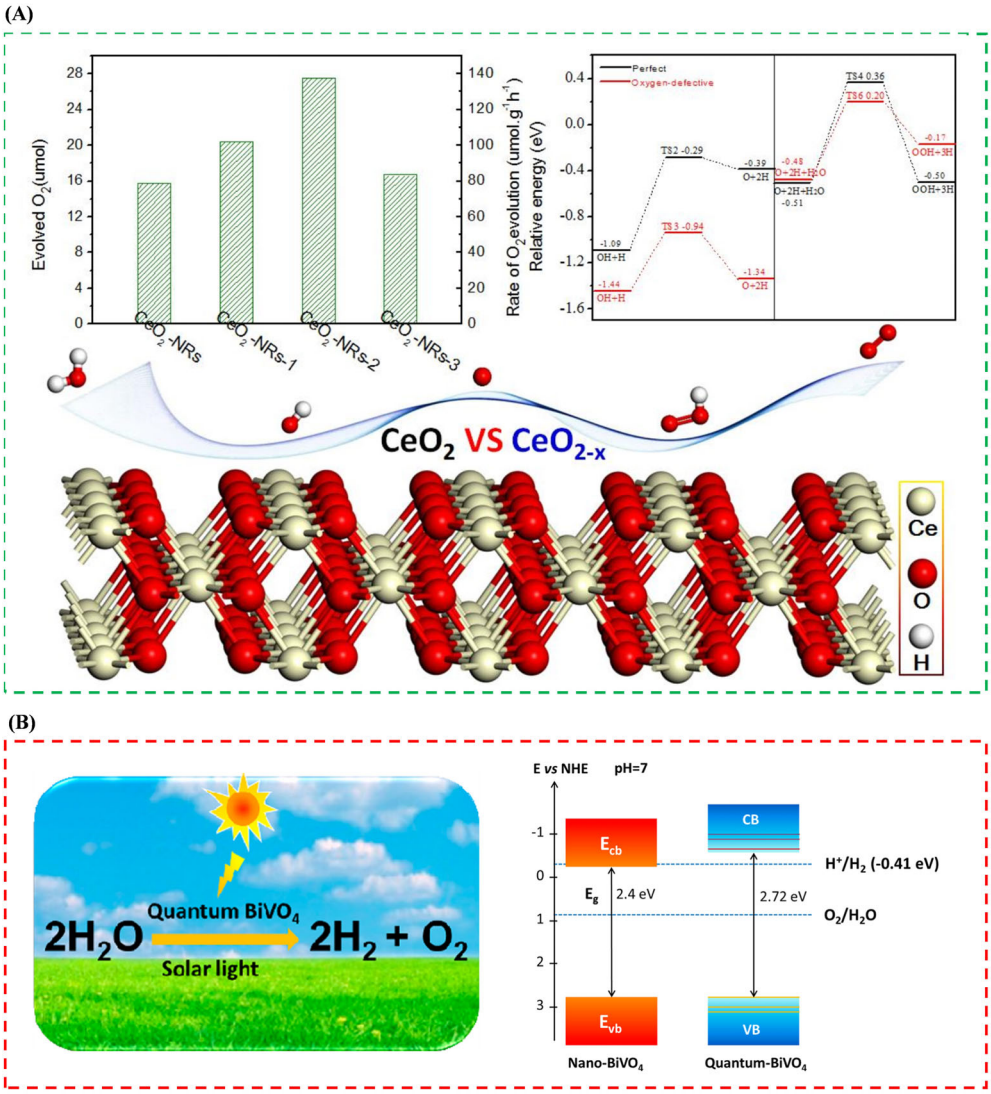

FIGURE 13 A, The role of oxygen vacancies in photocatalytic water oxidation on CeO_2. B, Schematic of band structures in nano-$BiVO_4$ and quantum-$BiVO_4$. *Source*: A, Reproduced with permission: Copyright 2018, Elsevier.[222] *Source*: B, Reproduced with permission: Copyright 2014, American Chemical Society[223]

$BiVO_4$ which can achieve the water decomposition into H_2 and O_2 without any co-catalyst or sacrificial reagent under the simulated sunlight irradiation (Figure 13B). The quantum-sized $BiVO_4$ has almost the same valence band edge position as the nanoscale sample, which may have a similar water oxidation potential. According to the UV-visible diffuse reflection spectra, the difference value of band gap between nanoscale $BiVO_4$ and quantum-size $BiVO_4$ is about 0.3 eV. Since the valence band position is almost the same, the negative displacement of conduction band position of quantum-size $BiVO_4$ may be greater than 0.1 eV. But their detailed mechanism for breaking down water has not been explained.[223]

5.2.3 | Photocatalytic nitrogen fixation

All organisms need nitrogen to make proteins, nucleic acids and many other biomolecules. However, N_2 molecular form in atmosphere is unusable for most organisms due to strong nonpolar N-N covalent bond towards dissociation, high ionization energy, negative electron affinity etc.[179,224] Therefore, it is a viable strategy by transforming N_2 in the atmosphere into the fully reduced form of ammonia (NH_3) that can be used by organisms. Thermodynamically, N_2 fixation is perfectly accessible ($N_{2(g)} + 3H_{2(g)} \rightarrow 2NH_{3(g)}$, $\Delta H_{298\ K} = -92.22$ kJ/mol), but it does not occur spontaneously under ambient conditions. Which can be explained to some extent via the stubborn triple bond of N_2 toward dissociation (944 kJ/mol) while kinetic inertia of N_2 might also be more related.[224,225] According to thermodynamic analyses, the fixation of N_2 on NH_3 does not consume energy itself, but the kinetic route determines the chemical inertness of N_2 in essence. Similar with biological N_2 fixation, photocatalytic N_2 fixation can be carried out under mild conditions through continuous self-excited electrons and water proton transfer. Therefore, photocatalytic nitrogen fixation including Bi-

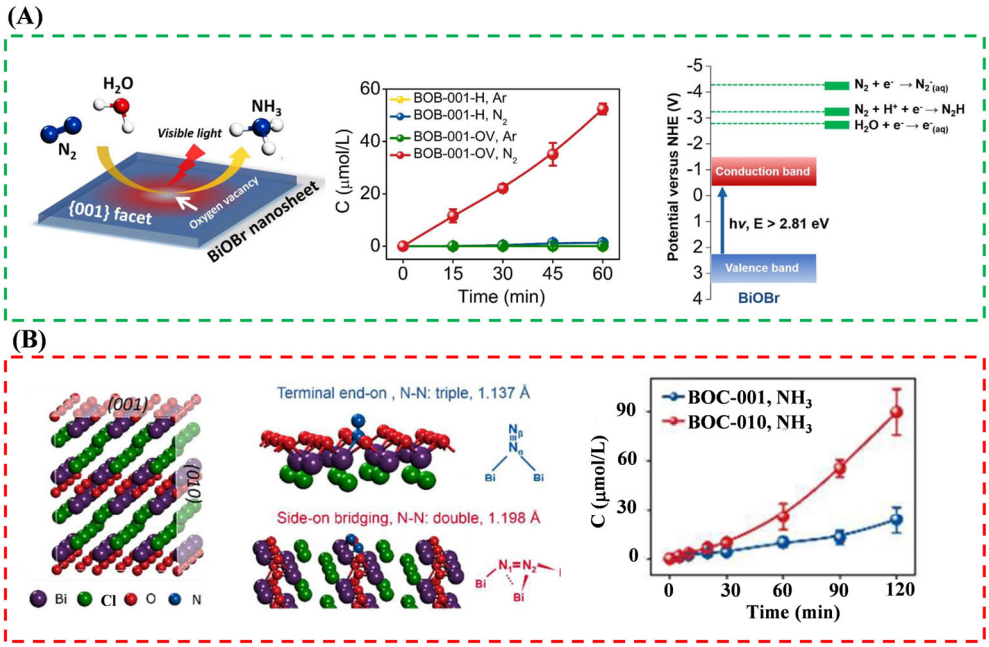

FIGURE 14 A, Photocatalytic fixation of N2 on BiOBr. B, N_2 adsorption and fixation on the {001} and {010} facets of BiOCl, quantitative determination of the generated NH_3. *Source*: A, Reproduced with permission: Copyright 2015, American Chemical Society.[179] *Source*: B, Reproduced with permission: Copyright 2015, Royal Society of Chemistry[225]

based photocatalysts has attracted the attention of scholars in recent years. Zhang et al demonstrate that the BiOBr nanosheets with oxygen vacancies can achieve efficient photocatalytic N2 fixation to NH3 without any organic scavengers and precious-metal cocatalysts under room temperature (Figure 14A).[179] Zhang et al point out that OVs of BiOCl can be as the active sites to build lower energy molecular steps, which are amendable for the N-N triple bond cleavage via a proton-assisted electron transfer pathway under light irradiation (Figure 14B). Therefore, that would overcome the kinetic inertia of N_2. Additionally, the N_2 fixation pathways would be determined by the distinguishing structures on different BiOCl facets with OVs, which would influence N_2 adsorption and activation. For the OVs of BiOCl {001} facets, the fixation of terminal end on bound N_2 follows an asymmetric distal pattern by selectively generating NH_3 (Figure 14B).[225]

5.2.4 | Summary discussion

Based on the researches of Bi-based photocatalysts in the field of energy catalysis, it can be seen that they have potential application prospects. In the process of energy conversion by using photocatalysis, the conductance potential of semiconductor photocatalysts and highly separated electrons will play an important role. In general, the conduction band potential requires a reduction potential that corresponds to the reduction reaction in order to facilitate the reaction. Combined with the structural adjustment strategy in Section 3, the position of the conduction band in the energy band structure can be adjusted by doping specific elements, so as to realize the matching of the conduction band potential and the reaction potential. In addition, the construction of heterojunctions can effectively realize the separation of photogenerated electrons and holes, thus promoting more photogenerated electrons to participate in the reduction reaction. Additionally, the selectivity of the reduction product may be controlled by adjusting the different conduction band potentials. Of course, the performance of photocatalytic reduction is also related to the adsorption and activation between catalyst and reactant molecules. Therefore, combined with the modification strategy in Section 3, the strategies of controlling morphology, crystal surface, metal deposition and design defects may provide effective adsorption and reaction sites. Therefore, the structural adjustment of bismuth-based semiconductors in the field of energy conversion can effectively improve the reducing properties of catalysts and determine their final reaction performance.

6 | CONCLUSION AND PROSPECTS

Due to its unique geometric structure, tunable electronic structure and decent visible light photocatalytic activity, Bi-based photocatalytic materials have broad application prospects in the field of environmental purification and clean energy development. At present, Bi-based nanomaterials are mostly studied as bismuth, bismuth oxide, bismuth oxyhalogen and bismuthate, which can be used as independent photocatalysts for environmental purification and energy development. However, their

photocatalysis efficiency is not ideal. Therefore, the modification of Bi-based photocatalyst has become one of the key directions. This review summarizes recent advances that researchers at home and abroad have made on the modification of Bi-based photocatalytic materials for improved photocatalytic properties. The strategies of metal/nonmetal doping, construction of heterojunctions, regulation of crystal facet exposure, and structural defects engineering have been discussed in detail. The optimized design of Bi-based photocatalytic materials shows excellent performance in typical applications in purification of air pollutants, photocatalytic degradation of liquid phase pollutants, reduction of CO_2, splitting of water to hydrogen, and demonstrated great potential in solar driven fields.

However, the optimization and modification of Bi-based photocatalytic materials are still in the laboratory. The researchers have not fully understood the structure-activity relationship among material microstructure, photocatalytic performance and reaction mechanism. They still need to further combine experiments and theoretical calculation to further explore the reaction mechanisms at the molecular and atomic levels, so as to provide a solid basis for the design of new Bi-based photocatalytic materials with specific functions. In addition, the current research work has not completely solved the problem of low efficiency on Bi-based photocatalysts in the utilization of sunlight. How to expand the range of light absorption response and improve the photon utilization rate are the areas that researchers need to study and improve in the future. Also, some Bi-based photocatalytic materials are easy to be poisoned and inactivated in practical application. So, how to improve the stability of bismuth photocatalytic materials, product selectivity and how to inhibit toxic by-products will be the important research directions in the development of efficient and stable photocatalysts. The challenges of Bi-based photocatalytic materials also lie in the identification of the active sites and the dynamic reconstruction of surface structure under light irradiation. To solve these issues, advanced in situ technique should be developed and applied to monitor the surface state under working conditions.

While challenges and pitfalls still exist in this important area, we are optimistic that with the deep integration of experimental research, computational investigation, and in situ characterization technique, novel efficient Bi-based photocatalytic materials can be developed in the near future and the new mechanistic understanding of the reaction mechanism will be advanced. We hope this review can provide some solid references to the recent advances and, more importantly, inspire future research in this emergent field.

ACKNOWLEDGMENTS

This work was supported by the National Natural Science Foundation of China (21822601 and 21777011), the 111 Project (B20030), The Graduate Research Innovation Fund Project of Southwest Petroleum University (2019cxyb012). The Plan for "National Youth Talents" of the Organization Department of the Central Committee, the Graduate Research and Innovation Foundation of Chongqing (CYS18019).

ORCID

Fan Dong https://orcid.org/0000-0003-2890-9964

REFERENCES

1. Peter SC. Reduction of CO_2 to chemicals and fuels: a solution to global warming and energy crisis. *ACS Energy Lett*. 2018;3:1557-1561.
2. Li M, Liu Y, Dong L, et al. Recent advances on photocatalytic fuel cell for environmental applications—the marriage of photocatalysis and fuel cells. *Sci Total Environ*. 2019;668:966-978.
3. Mamba G, Mishra AK. Graphitic carbon nitride (g-C_3N_4) nanocomposites: a new and exciting generation of visible light driven photocatalysts for environmental pollution remediation. *Appl Catal B-Environ*. 2016;198:347-377.
4. Zhang Q, Xu EG, Li J, et al. A review of microplastics in table salt, drinking water, and air: direct human exposure. *Environ Sci Technol*. 2020;54:3740-3751.
5. Hisatomi T, Domen K. Reaction systems for solar hydrogen production via water splitting with particulate semiconductor photocatalysts. *Nat Catal*. 2019;2:387-399.
6. Carbajo J, Jiménez M, Miralles S, Malato S, Faraldos M, Bahamonde A. Study of application of titania catalysts on solar photocatalysis: influence of type of pollutants and water matrices. *Chem Eng J*. 2016;291:64-73.
7. Lang X, Zhao J, Chen X. Visible-light-induced photoredox catalysis of dye-sensitized titanium dioxide: selective aerobic oxidation of organic sulfides. *Angew Chem Int Ed*. 2016;55:4697-4700.
8. Li K, Peng B, Peng T. Recent advances in heterogeneous photocatalytic CO_2 conversion to solar fuels. *ACS Catal*. 2016;6:7485-7527.
9. Vikrant K, Kim K-H, Deep A. Photocatalytic mineralization of hydrogen sulfide as a dual-phase technique for hydrogen production and environmental remediation. *Appl Catal B-Environ*. 2019;259:118025.
10. Boyjoo Y, Sun H, Liu J, Pareek VK, Wang S. A review on photocatalysis for air treatment: from catalyst development to reactor design. *Chem Eng J*. 2017;310:537-559.
11. Takanabe K. Photocatalytic water splitting: quantitative approaches toward photocatalyst by design. *ACS Catal*. 2017;7:8006-8022.
12. Yang X, Wang D. Photocatalysis: from fundamental principles to materials and applications. *ACS Appl Energy Mater*. 2018;1:6657-6693.
13. Guo Q, Ma Z, Zhou C, Ren Z, Yang X. Single molecule photocatalysis on TiO_2 surfaces. *Chem Rev*. 2019;119:11020-11041.

14. Naldoni A, Altomare M, Zoppellaro G, et al. Photocatalysis with reduced TiO_2: from black TiO_2 to cocatalyst-free hydrogen production. *ACS Catal*. 2019;9:345-364.
15. Qin T, Zhang X, Wang D, et al. Oxygen vacancies boost δ-Bi_2O_3 as a high-performance electrode for rechargeable aqueous batteries. *ACS Appl Mater Interfaces*. 2019;11:2103-2111.
16. Dou W, Hu X, Kong L, Peng X. UV-improved removal of chloride ions from strongly acidic wastewater using Bi_2O_3: efficiency enhancement and mechanisms. *Environ Sci Technol*. 2019;53:10371-10378.
17. Wang Z, Mi B. Environmental applications of 2D molybdenum disulfide (MoS_2) nanosheets. *Environ Sci Technol*. 2017;51:8229-8244.
18. Navalón S, Dhakshinamoorthy A, Álvaro M, Garcia H. Photocatalytic CO_2 reduction using non-titanium metal oxides and sulfides. *ChemSusChem*. 2013;6:562-577.
19. Parzinger E, Miller B, Blaschke B, et al. Photocatalytic stability of single- and few-layer MoS_2. *ACS Nano*. 2015;9:11302-11309.
20. Jin J, He T. Facile synthesis of Bi_2S_3 nanoribbons for photocatalytic reduction of CO_2 into CH_3OH. *Appl Surf Sci*. 2017;394:364-370.
21. Chahkandi M, Zargazi M. Novel method of square wave voltammetry for deposition of Bi_2S_3 thin film: photocatalytic reduction of hexavalent Cr in single and binary mixtures. *J Hazard Mater*. 2019;380:120879.
22. Zhang LW, Wang YJ, Cheng HY, Yao WQ, Zhu YF. Synthesis of porous Bi_2WO_6 thin films as efficient visible-light-active photocatalysts. *Adv Mater*. 2009;21:1286-1290.
23. Ouyang S, Tong H, Umezawa N, et al. Surface-alkalinization-induced enhancement of photocatalytic H_2 evolution over $SrTiO_3$-based photocatalysts. *J Am Chem Soc*. 2012;134:1974-1977.
24. Hsieh P-L, Naresh G, Huang Y-S, et al. Shape-tunable $SrTiO_3$ crystals revealing facet-dependent optical and photocatalytic properties. *J Phys Chem C*. 2019;123:13664-13671.
25. Yu H, Jiang L, Wang H, et al. Modulation of Bi_2MoO_6-based materials for photocatalytic water splitting and environmental application: a critical review. *Small*. 2019;15:1901008.
26. Shi Y, Hua C, Li B, et al. Highly ordered mesoporous crystalline $MoSe_2$ material with efficient visible-light-driven photocatalytic activity and enhanced lithium storage performance. *Adv Funct Mater*. 2013;23:1832-1838.
27. Xue H, Wang Y, Dai Y, et al. A $MoSe_2$/WSe_2 heterojunction-based photodetector at telecommunication wavelengths. *Adv Funct Mater*. 2018;28:1804388.
28. Choo S, Ban HW, Gu DH, et al. Synthesis of inorganic–organic 2D CdSe slab-diamine quantum nets. *Small*. 2019;15:1804426.
29. Fan X-B, Yu S, Wang X, et al. Susceptible surface sulfide regulates catalytic activity of CdSe quantum dots for hydrogen photogeneration. *Adv Mater*. 2019;31:1804872.
30. Sun M, Liu H, Qu J, Li J. Earth-rich transition metal phosphide for energy conversion and storage. *Adv Energy Mater*. 2016;6:1600087.
31. Prins R, Bussell ME. Metal phosphides: preparation, characterization and catalytic reactivity. *Catal Lett*. 2012;142:1413-1436.
32. Cao S, Wang C-J, Fu W-F, Chen Y. Metal phosphides as co-catalysts for photocatalytic and photoelectrocatalytic water splitting. *ChemSusChem*. 2017;10:4306-4323.
33. Kim S, Wang Y, Zhu M, Fujitsuka M, Majima T. Facet effects of Ag_3PO_4 on charge-carrier dynamics: trade-off between photocatalytic activity and charge-carrier lifetime. *Chem-Eur J*. 2018;24:14928-14932.
34. Li J, Zhang W, Ran M, Sun Y, Huang H, Dong F. Synergistic integration of Bi metal and phosphate defects on hexagonal and monoclinic $BiPO_4$: enhanced photocatalysis and reaction mechanism. *Appl Catal B-Environ*. 2019;243:313-321.
35. Khuzwayo Z, Chirwa EMN. The impact of alkali metal halide electron donor complexes in the photocatalytic degradation of pentachlorophenol. *J Hazard Mater*. 2017;321:424-431.
36. Wang H, Yang J, Li X, Zhang H, Li J, Guo L. Facet-dependent photocatalytic properties of AgBr nanocrystals. *Small*. 2012;8:2802-2806.
37. Kong W, Wang S, Wu D, et al. Fabrication of 3D sponge@AgBr-AgCl/ag and tubular photoreactor for continuous wastewater purification under sunlight irradiation. *ACS Sustain Chem Eng*. 2019;7:14051-14063.
38. Shi M, Li G, Li J, et al. Intrinsic facet-dependent reactivity of well-defined BiOBr nanosheets on photocatalytic water splitting. *Angew Chem Int Ed*. 2020;59:6590-6595.
39. Li J, Yu Y, Zhang L. Bismuth oxyhalide nanomaterials: layered structures meet photocatalysis. *Nanoscale*. 2014;6:8473-8488.
40. Sharma K, Dutta V, Sharma S, et al. Recent advances in enhanced photocatalytic activity of bismuth oxyhalides for efficient photocatalysis of organic pollutants in water: a review. *J Ind Eng Chem*. 2019;78:1-20.
41. Xie Y, Yang J, Chen Y, et al. Promising application of SiC without co-catalyst in photocatalysis and ozone integrated process for aqueous organics degradation. *Catal Today*. 2018;315:223-229.
42. Zhao ZW, Sun YJ, Dong F. Graphitic carbon nitride based nanocomposites: a review. *Nanoscale*. 2015;7:15-37.
43. Tang P, Hu G, Li M, Ma D. Graphene-based metal-free catalysts for catalytic reactions in the liquid phase. *ACS Catal*. 2016;6:6948-6958.
44. He R, Xu D, Cheng B, Yu J, Ho W. Review on nanoscale Bi-based photocatalysts. *Nanoscale Horiz*. 2018;3:464-504.
45. Yan X, Yuan K, Lu N, et al. The interplay of sulfur doping and surface hydroxyl in band gap engineering: mesoporous sulfur-doped TiO_2 coupled with magnetite as a recyclable, efficient, visible light active photocatalyst for water purification. *Appl Catal B-Environ*. 2017;218:20-31.
46. Kunioku H, Higashi M, Tomita O, et al. Strong hybridization between Bi-6s and O-2p orbitals in Sillén–Aurivillius perovskite Bi_4MO_8X (M = Nb, Ta; X = Cl, Br), visible light photocatalysts enabling stable water oxidation. *J Mater Chem A*. 2018;6:3100-3107.
47. Zhang Z, Wang W, Shang M, Yin W. Low-temperature combustion synthesis of Bi_2WO_6 nanoparticles as a visible-light-driven photocatalyst. *J Hazard Mater*. 2010;177:1013-1018.
48. Cheng H, Huang B, Dai Y. Engineering BiOX (X = Cl, Br, I) nanostructures for highly efficient photocatalytic applications. *Nanoscale*. 2014;6:2009-2026.

49. Wu CY, Sun L, Liang CP, Gong HR, Chang ML, Chen DC. Electronic structures and thermoelectric properties of polytype phases of bismuth. *J Phys Chem Solid*. 2019;134:52-57.
50. Cucka P, Barrett CS. The crystal structure of Bi and of solid solutions of Pb, Sn, Sb and Te in Bi. *Acta Crystallogr*. 1962;15:865-872.
51. Needs RJ, Martin RM, Nielsen OH. Total-energy calculations of the structural properties of the group-V element arsenic. *Phys Rev B Condens Matter*. 1986;33:3778-3784.
52. Hofmann P. The surfaces of bismuth: structural and electronic properties. *Prog Surf Sci*. 2006;81:191-245.
53. Shick AB, Ketterson JB, Novikov DL, Freeman AJ. Electronic structure, phase stability, and semimetal-semiconductor transitions in Bi. *Phys Rev B*. 1999;60:15484-15487.
54. Shu Y, Hu W, Liu Z, et al. Coexistence of multiple metastable polytypes in rhombohedral bismuth. *Sci Rep*. 2016;6:20337.
55. Fritz DM, Reis DA, Adams B, et al. Ultrafast bond softening in bismuth: mapping a solid' s interatomic potential with X-rays. *Science*. 2007;315:633-636.
56. Schiferl D, Barrett CS. The crystal structure of arsenic at 4.2, 78 and 299°K. *J Appl Cryst*. 1969;2:30-36.
57. Chen L, Wang Q, Xiong L, Gong H. Computationally predicted fundamental behaviors of embedded hydrogen at TiC/W interfaces. *Int J Hydrogen Energy*. 2018;43:16180-16186.
58. Gonze X, Michenaud J-P, Vigneron J-P. Ab initio calculations of bismuth properties, including spin–orbit coupling. *Phys Scr*. 1988;37:785-789.
59. Gonze X, Michenaud JP, Vigneron JP. First-principles study of As, Sb, and Bi electronic properties. *Phys Rev B Condens Matter*. 1990;41:11827-11836.
60. Gerlach E, Grosse P, Rautenberg M, Senske W. Dynamical conductivity and plasmon excitation in Bi. *Phys Status Solidi B*. 1976;75:553-558.
61. Dong F, Xiong T, Sun Y, et al. A semimetal bismuth element as a direct plasmonic photocatalyst. *Chem Commun*. 2014;50:10386-10389.
62. Yang FY, Liu K, Chien CL, Searson PC. Large magnetoresistance and finite-size effects in electrodeposited single-crystal bi thin films. *Phys Rev Lett*. 1999;82:3328-3331.
63. Zhang Q, Zhou Y, Wang F, et al. From semiconductors to semimetals: bismuth as a photocatalyst for NO oxidation in air. *J Mater Chem A*. 2014;2:11065-11072.
64. Yang FY, Liu K, Hong K, et al. Large magnetoresistance of electrodeposited single-crystal bismuth thin films. *Science*. 1999;284:1335-1337.
65. O'Brien B, Plaza M, Zhu LY, Perez L, Chien CL, Searson PC. Magnetotransport properties of electrodeposited bismuth films. *J Phys Chem C*. 2008;112:12018-12023.
66. Toudert J, Serna R, Jiménez de Castro M. Exploring the optical potential of nano-bismuth: tunable surface plasmon resonances in the near ultraviolet-to-near infrared range. *J Phys Chem C*. 2012;116:20530-20539.
67. McMahon JM, Schatz GC, Gray SK. Plasmonics in the ultraviolet with the poor metals Al, Ga, In, Sn, Tl, Pb, and Bi. *Phys Chem Chem Phys*. 2013;15:5415-5423.
68. Shuk P, Wiemhöfer HD, Guth U, et al. Oxide ion conducting solid electrolytes based on Bi_2O_3. *Solid State Ion*. 1996;89:179-196.
69. Drache M, Roussel P, Wignacourt J-P. Structures and oxide mobility in Bi−Ln−O materials: heritage of Bi_2O_3. *Chem Rev*. 2007;107:80-96.
70. Cabot A, Marsal A, Arbiol J, Morante JR. Bi_2O_3 as a selective sensing material for NO detection. *Sens Actuators B: Chem*. 2004;99:74-89.
71. Jiang N, Wachsman ED, Jung S-H. A higher conductivity Bi_2O_3-based electrolyte. *Solid State Ion*. 2002;150:347-353.
72. Leontie L, Caraman M, Delibaş M, Rusu GI. Optical properties of bismuth trioxide thin films. *Mater Res Bull*. 2001;36:1629-1637.
73. Walsh A, Watson GW, Payne DJ, et al. Electronic structure of the delta phases of Bi_2O_3: a combined ab initio and x-ray spectroscopy study. *Phys Rev B*. 2006;73:235104.
74. Qiu Y, Liu D, Yang J, Yang S. Controlled synthesis of bismuth oxide nanowires by an oxidative metal vapor transport deposition technique. *Adv Mater*. 2006;18:2604-2608.
75. Zhang L, Wang W, Yang J, et al. Sonochemical synthesis of nanocrystallite Bi_2O_3 as a visible-light-driven photocatalyst. *Appl Catal Gen*. 2006;308:105-110.
76. Uncovering the structural stabilities of the functional bismuth containing oxides: a case study of α-Bi_2O_3 nanoparticles in aqueous solutions. *New J Chem*. 2011;35:197.
77. Kinomura N, Kumada N. Preparation of bismuth oxides with mixed valence from hydrated sodium bismuth oxide. *Mater Res Bull*. 1995;30:129-134.
78. Kumada N, Kinomura N, Woodward PM, Sleight AW. Crystal structure of Bi_2O_4 with β-Sb_2O_4-type structure. *J Solid State Chem*. 1995;116:281-285.
79. Wang W, Chen X, Liu G, et al. Monoclinic dibismuth tetraoxide: a new visible-light-driven photocatalyst for environmental remediation. *Appl Catal B-Environ*. 2015;176-177:444-453.
80. Xia D, Wang W, Yin R, et al. Enhanced photocatalytic inactivation of *Escherichia coli* by a novel Z-scheme g-C_3N_4/m-Bi_2O_4 hybrid photocatalyst under visible light: the role of reactive oxygen species. *Appl Catal B-Environ*. 2017;214:23-33.
81. Ra H, Cao S, Zhou P, et al. Recent advances in visible light Bi-based photocatalysts. *Chin J Catal*. 2014;35:989-1007.
82. Tong W, Zhou X, Zhang H, et al. Bi_2S_3 nanostructures: a new photocatalyst. *Nano Res*. 2010;3:379-386.
83. Wang Y, Chen J, Wang P, Chen L, Chen YB, Wu LM. Syntheses, growth mechanism, and optical properties of [001] growing Bi_2S_3 nanorods. *J Phys Chem C*. 2009;113:16009-16014.
84. Liu Z, Peng S, Xie Q, et al. Large-scale synthesis of ultralong Bi_2S_3 nanoribbons via a solvothermal process. *Adv Mater*. 2010;15:936-940.
85. Liu X, Cui J, Zhang L, Yu W, Guo F, Qian Y. Control to synthesize Bi_2S_3 nanowires by a simple inorganic-surfactant-assisted solvothermal process. *Nanotechnology*. 2005;16:1771-1775.
86. Bhachu DS, Moniz SJA, Sathasivam S, et al. Bismuth oxyhalides: synthesis, structure and photoelectrochemical activity. *Chem Sci*. 2016;7:4832-4841.
87. Zhang KL, Liu CM, Huang FQ, et al. Study of the electronic structure and photocatalytic activity of the BiOCl photocatalyst. *Appl Catal B-Environ*. 2006;68:125-129.
88. Guan M, Xiao C, Zhang J, et al. Vacancy associates promoting solar-driven photocatalytic activity of ultrathin bismuth

oxychloride nanosheets. *J Am Chem Soc*. 2013;135:10411-10417.

89. Li K, Xu Y, He Y, Yang C, Wang Y, Jia J. Photocatalytic fuel cell (PFC) and dye self-photosensitization photocatalytic fuel cell (DSPFC) with BiOCl/Ti photoanode under UV and visible light irradiation. *Environ Sci Technol*. 2013;47:3490-3497.
90. Zhang L, Wang W, Sun S, Sun Y, Gao E, Xu J. Water splitting from dye wastewater: a case study of BiOCl/copper (II) phthalocyanine composite photocatalyst. *Appl Catal B-Environ*. 2013;132-133:315-320.
91. Yuan R, Fan S, Zhou H, et al. Chlorine-radical-mediated photocatalytic activation of C-H bonds with visible light. *Angew Chem Int Ed*. 2013;52:1035-1039.
92. Zhao L, Zhang X, Fan C, Liang Z, Han P. First-principles study on the structural, electronic and optical properties of BiOX (X=Cl, Br, I) crystals. *Phys B: Condensed Matter*. 2012;407:3364-3370.
93. Zhang H. First-principles studies on facet-dependent photocatalytic properties of bismuth oxyhalides (BiOXs). *RSC Adv*. 2012;2:9224-9229.
94. Wang W, Yang W, Chen R, et al. Investigation of band offsets of interface BiOCl:Bi_2WO_6: a first-principles study. *Phys Chem Chem Phys*. 2012;14:2450-2454.
95. Lim AR, Choh SH, Jang MS. Prominent ferroelastic domain walls in $BiVO_4$ crystal. *J Phys Condens Matter*. 1995;7:7309-7323.
96. Bierlein JD, Sleight AW. Ferroelasticity in $BiVO_4$. *Solid State Commun*. 1975;16:69-70.
97. Kudo A, Omori K, Kato H. A novel aqueous process for preparation of crystal form-controlled and highly crystalline $BiVO_4$ powder from layered vanadates at room temperature and its photocatalytic and photophysical properties. *J Am Chem Soc*. 1999;121:11459-11467.
98. Sleight AW, Chen H-Y, Ferretti A, Cox DE. Crystal growth and structure of $BiVO_4$. *Mater Res Bull*. 1979;14:1571-1581.
99. Yoneda Y, Kohara S, Takeda H, Tsurumi T. Local structure analysis of Bi_2WO_6. *Jpn J Appl Phys*. 2012;51:09LE06.
100. Mcdowell NA, Knight KS, Lightfoot P. Unusual high-temperature structural behavior in ferroelectric Bi_2WO_6. *Chemistry*. 2006;12:1493-1499.
101. Sun S, Wang W. Advanced chemical compositions and nanoarchitectures of bismuth based complex oxides for solar photocatalytic application. *RSC Adv*. 2014;4:47136-47152.
102. Huang H, Tian N, Jin S, Zhang Y, Wang S. Syntheses, characterization and nonlinear optical properties of a bismuth subcarbonate $Bi_2O_2CO_3$. *Solid State Sci*. 2014;30:1-5.
103. Ni Z, Sun Y, Zhang Y, Dong F. Fabrication, modification and application of $(BiO)_2CO_3$-based photocatalysts: a review. *Appl Surf Sci*. 2016;365:314-335.
104. Oshikiri M, Boero M, Ye J, Zou Z, Kido G. Electronic structures of promising photocatalysts $InMO_4$ (M=V, Nb, ta) and $BiVO_4$ for water decomposition in the visible wavelength region. *J Chem Phys*. 2002;117:7313-7318.
105. Zhao Z, Li Z, Zou Z. Electronic structure and optical properties of monoclinic clinobisvanite $BiVO_4$. *Phys Chem Chem Phys*. 2011;13:4746-4753.
106. Walsh A, Yan Y, Huda MN, al-Jassim MM, Wei SH. ChemInform abstract: band edge electronic structure of $BiVO_4$: elucidating the role of the Bi s and V d orbitals. *Chem Mater*. 2009;21:547-551.
107. Lai K, Wei W, Dai Y, Zhang R, Huang B. DFT calculations on structural and electronic properties of Bi_2MO_6(M = Cr, Mo, W). *Rare Metals*. 2011;30:166-172.
108. Fu H, Pan C, Yao W, Zhu Y. Visible-light-induced degradation of rhodamine B by nanosized Bi_2WO_6. *J Phys Chem B*. 2005;109:22432-22439.
109. Oshikiri M, Boero M. Water molecule adsorption properties on the $BiVO_4$ (100) surface. *J Phys Chem B*. 2006;110:9188-9194.
110. Zheng Y, Duan F, Chen M, Xie Y. Synthetic $Bi_2O_2CO_3$ nanostructures: novel photocatalyst with controlled special surface exposed. *J Mol Catal A: Chem*. 2010;317:34-40.
111. Huang H, Wang J, Dong F, et al. Highly efficient $Bi_2O_2CO_3$ single-crystal lamellas with dominantly exposed {001} facets. *Cryst Growth Des*. 2015;15:534-537.
112. Dong F, Ho W-K, Lee SC, et al. Template-free fabrication and growth mechanism of uniform $(BiO)_2CO_3$ hierarchical hollow microspheres with outstanding photocatalytic activities under both UV and visible light irradiation. *J Mater Chem*. 2011;21:12428-12436.
113. Liu Y, Wang Z, Huang B, et al. Preparation, electronic structure, and photocatalytic properties of $Bi_2O_2CO_3$ nanosheet. *Appl Surf Sci*. 2010;257:172-175.
114. Cheng H, Huang B, Lu J, et al. Synergistic effect of crystal and electronic structures on the visible-light-driven photocatalytic performances of Bi_2O_3 polymorphs. *Phys Chem Chem Phys*. 2010;12:15468-15475.
115. Chen X, Mao SS. Titanium dioxide nanomaterials: synthesis, properties, modifications, and applications. *Chem Rev*. 2007;107:2891-2959.
116. Osterloh FE. Inorganic nanostructures for photoelectrochemical and photocatalytic water splitting. *Chem Soc Rev*. 2013;42:2294-2320.
117. Zhang L, Wang W, Zhou L, Xu H. Bi_2WO_6 nano- and microstructures: shape control and associated visible-light-driven photocatalytic activities. *Small*. 2007;3:1618-1625.
118. Hagfeldt A, Graetzel M. Light-induced redox reactions in nanocrystalline systems. *Chem Rev*. 1995;95:49-68.
119. Ma D, Zhao J, Zhao Y, Hao XL, Lu Y. An easy synthesis of 1D bismuth nanostructures in acidic solution and their photocatalytic degradation of rhodamine B. *Chem Eng J*. 2012;209:273-279.
120. Wang Z, Jiang C, Huang R, Peng H, Tang X. Investigation of optical and photocatalytic properties of bismuth nanospheres prepared by a facile thermolysis method. *J Phys Chem C*. 2014;118:1155-1160.
121. Ma D, Zhao J, Chu R, et al. Novel synthesis and characterization of bismuth nano/microcrystals with sodium hypophosphite as reductant. *Adv Powder Technol*. 2013;24:79-85.
122. Ma D, Zhao J, Li Y, et al. Organic molecule directed synthesis of bismuth nanostructures with varied shapes in aqueous solution and their optical characterization. *Colloid Surf A*. 2010;368:105-111.
123. Obregón S, Caballero A, Colón G. Hydrothermal synthesis of $BiVO_4$: structural and morphological influence on the photocatalytic activity. *Appl Catal B-Environ*. 2012;117-118:59-66.

124. Zhang L, Wang H, Chen Z, et al. Bi_2WO_6 micro/nano-structures: synthesis, modifications and visible-light-driven photocatalytic applications. *Appl Catal B-Environ*. 2011;106:1-13.
125. Zhang L, Wang W, Chen Z, Zhou L, Xu H, Zhu W. Fabrication of flower-like Bi_2WO_6 superstructures as high performance visible-light driven photocatalysts. *J Mater Chem*. 2007; 17:2526-2532.
126. Shang M, Wang W, Sun S, Zhou L, Zhang L. Bi_2WO_6 nanocrystals with high photocatalytic activities under visible light. *J Phys Chem C*. 2008;112:10407-10411.
127. Xia J, Li H, Luo Z, et al. Self-assembly and enhanced optical absorption of Bi_2WO_6 nests via ionic liquid-assisted hydrothermal method. *Mater Chem Phys*. 2010;121:6-9.
128. Wang C, Zhang H, Li F, Zhu L. Degradation and mineralization of bisphenol A by mesoporous Bi_2WO_6 under simulated solar light irradiation. *Environ Sci Technol*. 2010;44:6843-6848.
129. Fu H, Zhang L, Yao W, Zhu Y. Photocatalytic properties of nanosized Bi_2WO_6 catalysts synthesized via a hydrothermal process. *Appl Catal B-Environ*. 2006;66:100-110.
130. Zhang H, Yang Y, Zhou Z, Zhao Y, Liu L. Enhanced photocatalytic properties in BiOBr nanosheets with dominantly exposed (102) facets. *J Phys Chem C*. 2014;118:14662-14669.
131. Chen P, Sun Y, Liu H, et al. Facet-dependent photocatalytic NO conversion pathways predetermined by adsorption activation patterns. *Nanoscale*. 2019;11:2366-2373.
132. Ye L, Zan L, Tian L, Peng T, Zhang J. The {001} facets-dependent high photoactivity of BiOCl nanosheets. *Chem Commun*. 2011;47:6951-6953.
133. Norris DJ, Efros AL, Erwin SC. Doped nanocrystals. *Science*. 2008;319:1776-1779.
134. Liu G, Wang L, Yang HG, Cheng HM, (Max) Lu GQ. Titania-based photocatalysts—crystal growth, doping and heterostructuring. *J Mater Chem*. 2010;20:831-843.
135. Asahi R, Morikawa T, Ohwaki T, Aoki K, Taga Y. Visible-light photocatalysis in nitrogen-doped titanium oxides. *Science*. 2001;293:269-271.
136. Zhao W, Ma W, Chen C, Zhao J, Shuai Z. Efficient degradation of toxic organic pollutants with $Ni_2O_3/TiO_{2-x}B_x$ under visible irradiation. *J Am Chem Soc*. 2004;126:4782-4783.
137. Hu T, Li H, Du N, et al. Iron-doped bismuth tungstate with an excellent photocatalytic performance. *ChemCatChem*. 2018;10:3040-3048.
138. Zhou S, Zhang Q, Zhao D, et al. Synthesis, properties and mechanism of photodegradation of core–shell structured upconversion luminescent $NaYF_4:Yb^{3+},Er^{3+}$@BiOCl. *Appl Organomet Chem*. 2018;32:e4230.
139. He B, Li Z, Zhao D, et al. Fabrication of porous cu-doped $BiVO_4$ nanotubes as efficient oxygen-evolving photocatalysts. *ACS Appl Nano Mater*. 2018;1:2589-2599.
140. Regmi C, Kshetri YK, Kim T-H, Pandey RP, Lee SW. Visible-light-induced Fe-doped $BiVO_4$ photocatalyst for contaminated water treatment. *Mol Catal*. 2017;432:220-231.
141. Merupo VI, Velumani S, Oza G, et al. High energy ball-milling synthesis of nanostructured ag-doped and $BiVO_4$-based photocatalysts. *ChemistrySelect*. 2016;1:1278-1286.
142. Kong L, Jiang Z, Lai HHC, Xiao T, Edwards PP. Does noble metal modification improve the photocatalytic activity of BiOCl? *Prog Nat Sci: Mater Int*. 2013;23:286-293.
143. Dong F, Li Q, Sun Y, Ho WK. Noble metal-like behavior of plasmonic Bi particles as a cocatalyst deposited on $(BiO)_2CO_3$ microspheres for efficient visible light photocatalysis. *ACS Catal*. 2014;4:4341-4350.
144. Huang Y, Kang S, Yang Y, et al. Facile synthesis of Bi/Bi_2WO_6 nanocomposite with enhanced photocatalytic activity under visible light. *Appl Catal B-Environ*. 2016;196:89-99.
145. Zai J, Cao F, Liang N, et al. Rose-like I-doped $Bi_2O_2CO_3$ microspheres with enhanced visible light response: DFT calculation, synthesis and photocatalytic performance. *J Hazard Mater*. 2017;321:464-472.
146. Zheng H, Guo W, Li S, et al. Surfactant (CTAB) assisted flower-like Bi_2WO_6 through hydrothermal method: unintentional bromide ion doping and photocatalytic activity. *Catal Commun*. 2017;88:68-72.
147. Wu D, Yue S, Wang W, et al. Boron doped BiOBr nanosheets with enhanced photocatalytic inactivation of *Escherichia coli*. *Appl Catal B-Environ*. 2016;192:35-45.
148. Huang H, Li X, Wang J, et al. Anionic group self-doping as a promising strategy: band-gap engineering and multifunctional applications of high-performance CO_3^{2-}-doped $Bi_2O_2CO_3$. *ACS Catal*. 2015;5:4094-4103.
149. Parmar KPS, Kang HJ, Bist A, Dua P, Jang JS, Lee JS. Photocatalytic and photoelectrochemical water oxidation over metal-doped monoclinic $BiVO_4$ photoanodes. *ChemSusChem*. 2012;5:1926-1934.
150. Jo WJ, Jang J-W, Kong K-J, et al. Phosphate doping into monoclinic $BiVO_4$ for enhanced Photoelectrochemical water oxidation activity. *Angew Chem Int Ed*. 2012;51:3147-3151.
151. Marschall R. Semiconductor composites: strategies for enhancing charge carrier separation to improve photocatalytic activity. *Adv Funct Mater*. 2014;24:2421-2440.
152. Low J, Yu J, Jaroniec M, Wageh S, al-Ghamdi AA. Heterojunction photocatalysts. *Adv Mater*. 2017;29:1601694.
153. Wang H, Zhang L, Chen Z, et al. Semiconductor heterojunction photocatalysts: design, construction, and photocatalytic performances. *Chem Soc Rev*. 2014;43:5234-5244.
154. Wang S, Yun JH, Luo B, et al. Recent progress on visible light responsive heterojunctions for photocatalytic applications. *J Mater Sci Technol*. 2017;33:1-22.
155. Zhou H, Qu Y, Zeid T, Duan X. Towards highly efficient photocatalysts using semiconductor nanoarchitectures. *Energy Environ Sci*. 2012;5:6732-6743.
156. Wang Y, Wang Q, Zhan X, Wang F, Safdar M, He J. Visible light driven type II heterostructures and their enhanced photocatalysis properties: a review. *Nanoscale*. 2013;5:8326-8339.
157. Eschbach M, Młyńczak E, Kellner J, et al. Realization of a vertical topological p–n junction in epitaxial Sb_2Te_3/Bi_2Te_3 heterostructures. *Nat Commun*. 2015;6:8816.
158. Weng B, Xu F, Xu J. Synthesis of hierarchical $Bi_2O_3/Bi_4Ti_3O_{12}$ p-n junction nanoribbons on carbon fibers from (001) facet dominated TiO_2 nanosheets. *RSC Adv*. 2014;4:56682-56689.
159. Zhang W, Xa D, Jia B, et al. 2D $BiOCl/Bi_{12}O_{17}Cl_2$ nanojunction: enhanced visible light photocatalytic NO removal and in situ DRIFTS investigation. *Appl Surf Sci*. 2018;430:571-577.
160. Huang H, Xiao K, He Y, et al. In situ assembly of $BiOI@Bi_{12}O_{17}Cl_2$ p-n junction: charge induced unique front-lateral surfaces coupling heterostructure with high exposure

of BiOI {001} active facets for robust and nonselective photocatalysis. *Appl Catal B-Environ*. 2016;199:75-86.

161. He Z, Shi Y, Gao C, Wen L, Chen J, Song S. BiOCl/$BiVO_4$ p–n heterojunction with enhanced photocatalytic activity under visible-light irradiation. *J Phys Chem C*. 2014;118:389-398.
162. Zou X, Dong Y, Zhang X, Cui Y, Ou X, Qi X. The highly enhanced visible light photocatalytic degradation of gaseous o-dichlorobenzene through fabricating like-flowers $BiPO_4$/BiOBr p-n heterojunction composites. *Appl Surf Sci*. 2017;391:525-534.
163. Yi J, Jiao C, Mo H, Chen Q, She Q, Li Z. In situ synthesis of Bi_2O_3/Bi_2MoO_6 heterostructured microspheres for efficiently removal of acid orange 7. *Ceram Int*. 2018;44:22102-22107.
164. Low J, Jiang C, Cheng B, Wageh S, al-Ghamdi AA, Yu J. A review of direct Z-scheme photocatalysts. *Small Methods*. 2017;1:1700080.
165. Ye L, Liu J, Gong C, Tian L, Peng T, Zan L. Two different roles of metallic Ag on Ag/AgX/BiOX (X = Cl, Br) visible light photocatalysts: surface plasmon resonance and Z-scheme bridge. *ACS Catal*. 2012;2:1677-1683.
166. Xiong T, Wen M, Dong F, et al. Three dimensional Z-scheme $(BiO)_2CO_3$/MoS_2 with enhanced visible light photocatalytic NO removal. *Appl Catal B-Environ*. 2016;199:87-95.
167. Zhou FQ, Fan JC, Xu QJ, Min YL. $BiVO_4$ nanowires decorated with CdS nanoparticles as Z-scheme photocatalyst with enhanced H_2 generation. *Appl Catal B-Environ*. 2017;201:77-83.
168. Wang S, Yang X, Zhang X, et al. A plate-on-plate sandwiched Z-scheme heterojunction photocatalyst: BiOBr-Bi_2MoO_6 with enhanced photocatalytic performance. *Appl Surf Sci*. 2017;391:194-201.
169. Yu J, Low J, Xiao W, Zhou P, Jaroniec M. Enhanced photocatalytic CO_2-reduction activity of anatase TiO_2 by coexposed {001} and {101} facets. *J Am Chem Soc*. 2014;136:8839-8842.
170. Tan HL, Wen X, Amal R, Ng YH. $BiVO_4$ {010} and {110} relative exposure extent: governing factor of surface charge population and photocatalytic activity. *J Phys Chem Lett*. 2016;7:1400-1405.
171. Di J, Chen C, Yang S-Z, et al. Defect engineering in atomically-thin bismuth oxychloride towards photocatalytic oxygen evolution. *J Mater Chem A*. 2014;2:4208-4216.
172. Zhang N, Li X, Ye H, et al. Oxide defect engineering enables to couple solar energy into oxygen activation. *J Am Chem Soc*. 2016;138:8928-8935.
173. Xiong J, Di J, Xia J, et al. Surface defect engineering in 2D nanomaterials for Photocatalysis. *Adv Funct Mater*. 2018;28:1801983.
174. Liu Y, Chong X, Zhou L, et al. Vacancy engineering for tuning electron and phonon structures of two-dimensional materials. *Adv Energy Mater*. 2016;6:1600436.
175. Li X, Zhang W, Cui W, et al. Reactant activation and photocatalysis mechanisms on Bi-metal@Bi_2GeO_5 with oxygen vacancies: a combined experimental and theoretical investigation. *Chem Eng J*. 2019;370:1366-1375.
176. Kong XY, Choo YY, Chai S-P, Soh AK, Mohamed AR. Oxygen vacancy induced Bi_2WO_6 for the realization of photocatalytic CO_2 reduction over the full solar spectrum: from the UV to the NIR region. *Chem Commun*. 2016;52:14242-14245.
177. Jin X, Lv C, Zhou X, et al. Molecular adsorption promotes carrier migration: key step for molecular oxygen activation of defective $Bi_4O_5I_2$. *Appl Catal B-Environ*. 2018;226:53-60.
178. Xu B, Gao Y, Li Y, et al. Synthesis of Bi_3O_4Cl nanosheets with oxygen vacancies: the effect of defect states on photocatalytic performance. *Appl Surf Sci*. 2020;507:144806.
179. Li H, Shang J, Ai Z, Zhang L. Efficient visible light nitrogen fixation with BiOBr nanosheets of oxygen vacancies on the exposed {001} facets. *J Am Chem Soc*. 2015;137:6393-6399.
180. Li H, Shang J, Yang Z, Shen W, Ai Z, Zhang L. Oxygen vacancy associated surface Fenton chemistry: surface structure dependent hydroxyl radicals generation and substrate dependent reactivity. *Environ Sci Technol*. 2017;51:5685-5694.
181. Li H, Qin F, Yang Z, Cui X, Wang J, Zhang L. New reaction pathway induced by plasmon for selective benzyl alcohol oxidation on BiOCl possessing oxygen vacancies. *J Am Chem Soc*. 2017;139:3513-3521.
182. Di J, Chen C, Zhu C, et al. Bismuth vacancy mediated single unit cell Bi_2WO_6 nanosheets for boosting photocatalytic oxygen evolution. *Appl Catal B-Environ*. 2018;238:119-125.
183. Gao S, Gu B, Jiao X, et al. Highly efficient and exceptionally durable CO_2 photoreduction to methanol over freestanding defective single-unit-cell bismuth vanadate layers. *J Am Chem Soc*. 2017;139:3438-3445.
184. Hoffmann MR, Martin ST, Choi W, Bahnemann DW. Environmental applications of semiconductor photocatalysis. *Chem Rev*. 1995;95:69-96.
185. Kale MJ, Avanesian T, Christopher P. Direct photocatalysis by plasmonic nanostructures. *ACS Catal*. 2014;4:116-128.
186. Christopher P, Xin H, Marimuthu A, Linic S. Singular characteristics and unique chemical bond activation mechanisms of photocatalytic reactions on plasmonic nanostructures. *Nat Mater*. 2012;11:1044-1050.
187. Warren SC, Thimsen E. Plasmonic solar water splitting. *Energ Environ Sci*. 2012;5:5133-5130.
188. Sun Y, Zhao Z, Dong F, Zhang W. Mechanism of visible light photocatalytic NOx oxidation with plasmonic Bi cocatalyst-enhanced $(BiO)_2CO_3$ hierarchical microspheres. *Phys Chem Chem Phys*. 2015;17:10383-10390.
189. Dong F, Xiong T, Yan S, et al. Facets and defects cooperatively promote visible light plasmonic photocatalysis with Bi nanowires@BiOCl nanosheets. *J Catal*. 2016;344:401-410.
190. Zhao Z, Zhang W, Sun Y, et al. Bi Cocatalyst/Bi_2MoO_6 microspheres nanohybrid with SPR-promoted visible-light photocatalysis. *J Phys Chem C*. 2016;120:11889-11898.
191. Wang H, Zhang W, Li X, et al. Highly enhanced visible light photocatalysis and in situ FT-IR studies on Bi metal@defective BiOCl hierarchical microspheres. *Appl Catal B-Environ*. 2018;225:218-227.
192. Xa D, Zhang W, Sun Y, et al. Visible-light-induced charge transfer pathway and photocatalysis mechanism on Bi semimetal@defective BiOBr hierarchical microspheres. *J Catal*. 2018;357:41-50.
193. Chen P, Liu H, Sun Y, et al. Bi metal prevents the deactivation of oxygen vacancies in $Bi_2O_2CO_3$ for stable and efficient photocatalytic NO abatement. *Appl Catal B-Environ*. 2020;264:118545.

194. Huang H, He Y, He R, et al. Novel Bi-based iodate photocatalysts with high photocatalytic activity. *Inorg Chem Commun*. 2014;40:215-219.
195. Jin X, Ye L, Xie H, Chen G. Bismuth-rich bismuth oxyhalides for environmental and energy photocatalysis. *Coord Chem Rev*. 2017;349:84-101.
196. He R, Xu D, Cheng B, Yu J, Ho W. Review on nanoscale bi-based photocatalyst. *Nanoscale Horiz*. 2018;3:464-504.
197. Kreuzer LB, Patel CKN. Nitric oxide air pollution: detection by optoacoustic spectroscopy. *Science*. 1971;173:45-47.
198. Jose G, Javier M-G, Ambuj S, et al. Household air pollution, health, and climate change: cleaning the air. *Environ Res Lett*. 2018;13:030201.
199. Yang X, Li C. Industrial environmental efficiency, foreign direct investment and export——evidence from 30 provinces in China. *J Clean Prod*. 2019;212:1490-1498.
200. Liu H, Chen P, Yuan X, et al. Pivotal roles of artificial oxygen vacancies in enhancing photocatalytic activity and selectivity on $Bi_2O_2CO_3$ nanosheets. *Chin J Catal*. 2019;40:620-630.
201. Li X, Zhang W, Li J, et al. Transformation pathway and toxic intermediates inhibition of photocatalytic NO removal on designed Bi metal@defective $Bi_2O_2SiO_3$. *Appl Catal B-Environ*. 2019;241:187-195.
202. Li J, Cui W, Chen P, et al. Unraveling the mechanism of binary channel reactions in photocatalytic formaldehyde decomposition for promoted mineralization. *Appl Catal B-Environ*. 2020;260:118130.
203. Wang Y, He Y, Li T, Cai J, Luo M, Zhao L. Photocatalytic degradation of methylene blue on $CaBi_6O_{10}/Bi_2O_3$ composites under visible light. *Chem Eng J*. 2012;189-190:473-481.
204. Phuruangrat A, Maneechote A, Dumrongrojthanath P, Ekthammathat N, Thongtem S, Thongtem T. Visible-light driven photocatalytic degradation of rhodamine B by Ag/Bi_2WO_6 heterostructures. *Mater Lett*. 2015;159:289-292.
205. Jiang Z, Yang F, Yang G, et al. The hydrothermal synthesis of BiOBr flakes for visible-light-responsive photocatalytic degradation of methyl orange. *J Photochem Photobiol A*. 2010;212:8-13.
206. Liu T, Zhang X, Zhao F, Wang Y. Targeting inside charge carriers transfer of photocatalyst: selective deposition of Ag_2O on $BiVO_4$ with enhanced UV–vis-NIR photocatalytic oxidation activity. *Appl Catal B-Environ*. 2019;251:220-228.
207. Chatterjee A, Kar P, Wulferding D, Lemmens P, Pal SK. Flower-like BiOI microspheres decorated with plasmonic gold nanoparticles for dual detoxification of organic and inorganic water pollutants. *ACS Appl Nano Mater*. 2020;3:2733-2744.
208. Yu S, Huang H, Dong F, et al. Synchronously achieving plasmonic bi metal deposition and I– doping by utilizing $BiOIO_3$ as the self-sacrificing template for high-performance multifunctional applications. *ACS Appl Mater Interfaces*. 2015;7:27925-27933.
209. Xiang Y, Ju P, Wang Y, Sun Y, Zhang D, Yu J. Chemical etching preparation of the Bi_2WO_6/BiOI p–n heterojunction with enhanced photocatalytic antifouling activity under visible light irradiation. *Chem Eng J*. 2016;288:264-275.
210. Duren RM, Miller CE. Measuring the carbon emissions of megacities. *Nat Clim Change*. 2012;2:560-562.
211. Lim XZ. How to make the most of carbon dioxide. *Nature*. 2015;526:628-630.
212. Katey WA, Thomas SD, Ingmar N, et al. 21st-century modeled permafrost carbon emissions accelerated by abrupt thaw beneath lakes. *Nat Commun*. 2018;9:3262.
213. Ma Z, Li P, Ye L, et al. Oxygen vacancies induced exciton dissociation of flexible BiOCl nanosheets for effective photocatalytic CO_2 conversion. *J Mater Chem A*. 2017;5:24995-25004.
214. Ye L, Su Y, Jin X, Xie H, Zhang C. Recent advances in BiOX (X = Cl, Br and I) photocatalysts: synthesis, modification, facet effects and mechanisms. *Environ Sci Nano*. 2014;1:90-112.
215. Li H, Li J, Jia FL, Zhang LZ. Oxygen vacancy-mediated photocatalysis of BiOCl: reactivity, selectivity, and perspectives. *Angew Chem*. 2018;57:122-138.
216. Ye L, Deng Y, Wang L, Xie H, Su F. Bismuth-based photocatalysts for solar photocatalytic carbon dioxide conversion. *ChemSusChem*. 2019;12:3671-3701.
217. Ye L, Jin X, Liu C, et al. Thickness-ultrathin and bismuth-rich strategies for BiOBr to enhance photoreduction of CO_2 into solar fuels. *Appl Catal B-Environ*. 2016;187:281-290.
218. Ye L, Jin X, Ji X, et al. Facet-dependent photocatalytic reduction of CO_2 on BiOI nanosheets. *Chem Eng J*. 2016;291:39-46.
219. Wang Z, Li C, Domen K. Recent developments in heterogeneous photocatalysts for solar-driven overall water splitting. *Chem Soc Rev*. 2019;48:2109-2125.
220. Maeda K, Domen K. Photocatalytic water splitting: recent progress and future challenges. *J PhysChemLett*. 2010;1:2655-2661.
221. Zhang L, Han Z, Wang W, et al. Solar-light-driven pure water splitting with ultrathin BiOCl nanosheets. *Chem Eur J*. 2015;21:18089-18094.
222. Zhang Y-C, Li Z, Zhang L, et al. Role of oxygen vacancies in photocatalytic water oxidation on ceria oxide: experiment and DFT studies. *Appl Catal B-Environ*. 2018;224:101-108.
223. Sun S, Wang W, Li D, Zhang L, Jiang D. Solar light driven pure water splitting on quantum sized $BiVO_4$ without any cocatalyst. *ACS Catal*. 2014;4:3498-3503.
224. Shilov AE. Catalytic reduction of molecular nitrogen in solutions. *Russ Chem Bull*. 2003;52:2555-2562.
225. Zhang LZ, Li H, Shang J, et al. Facet-dependent solar ammonia synthesis of BiOCl nanosheets via a proton-assisted electron transfer pathway. *Nanoscale*. 2015;8:1986-1993.

AUTHOR BIOGRAPHIES

Peng Chen received his MS in the College of Environment and Resources form Chongqing Technology and Business University in 2019. Currently, he is a PhD student at School of New Energy and Materials from Southwest Petroleum University. He focuses on the design of new materials for environmental and energy catalysis, mechanism research of reaction process and regulation of toxic by-products.

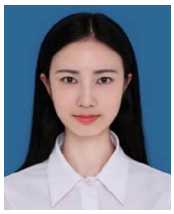

Hongjing Liu received her MS in the College of Environment and Ecology form Chongqing University in 2020. She focuses on the reaction mechanism of pollutant purification via using photocatalytic technology.

Li'ao Wang received her PhD at Chongqing University in 2001. Currently, she is a professor at the College of Environment and Ecology from Chongqing University. She is an expert with special state Council allowances, vice chairman of solid waste Special Committee of Chongqing Environmental Society, expert of the National Database of Science and Technology Experts, expert of Chongqing Eco-Environment expert database. She focuses on solid waste pollution control and recycling.

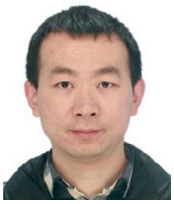

Fan Dong received her PhD at Zhejiang University in 2010. Currently, he is a professor and doctoral supervisor at the Institute of Foundation and Frontier Research from University of Electronic Science and Technology of China. He was selected as one of the top youth talents of the National "ten Thousand Talents Plan," winner of the National Science Fund for Outstanding Youth and expert of special Allowance of the State Council. He focuses on Environmental and energy catalytic materials, air pollution control technology, environmental chemistry, and material simulation, and so forth.

How to cite this article: Chen P, Liu H, Cui W, Lee SC, Wang L, Dong F. Bi-based photocatalysts for light-driven environmental and energy applications: Structural tuning, reaction mechanisms, and challenges. *EcoMat*. 2020;2: e12047. https://doi.org/10.1002/eom2.12047